

A consensus estimate for the ice thickness distribution of all glaciers on Earth

Daniel Farinotti^{1,2*}, Matthias Huss^{1,3}, Johannes J. Fürst⁴, Johannes Landmann^{1,2}, Horst Machguth^{3,5}, Fabien Maussion^{1,6} and Ankur Pandit^{7,8}

Knowledge of the ice thickness distribution of the world's glaciers is a fundamental prerequisite for a range of studies. Projections of future glacier change, estimates of the available freshwater resources or assessments of potential sea-level rise all need glacier ice thickness to be accurately constrained. Previous estimates of global glacier volumes are mostly based on scaling relations between glacier area and volume, and only one study provides global-scale information on the ice thickness distribution of individual glaciers. Here we use an ensemble of up to five models to provide a consensus estimate for the ice thickness distribution of all the about 215,000 glaciers outside the Greenland and Antarctic ice sheets. The models use principles of ice flow dynamics to invert for ice thickness from surface characteristics. We find a total volume of $158 \pm 41 \times 10^3 \text{ km}^3$, which is equivalent to $0.32 \pm 0.08 \text{ m}$ of sea-level change when the fraction of ice located below present-day sea level (roughly 15%) is subtracted. Our results indicate that High Mountain Asia hosts about 27% less glacier ice than previously suggested, and imply that the timing by which the region is expected to lose half of its present-day glacier area has to be moved forward by about one decade.

Glaciers and ice caps outside the Greenland and Antarctic ice sheets ('glaciers' in the following) are changing rapidly in response to climate change¹. Although they only contain a fraction of the worldwide ice volume², the consequences of their mass loss are widespread and of global significance: glacier changes affect global trends in freshwater availability^{3,4}, have dominated cryospheric contributions to recent sea level changes^{5,6} and are anticipated to affect regional water resources over the twenty-first century^{7,8}. Clearly, projections of such impacts require an estimate of the ice volume stored within present-day glaciers, and for regional-to local-scale projections the ice thickness distribution can also be essential^{9,10}. Recent studies showed that even small features in the bedrock topography can cause decadal-scale variations in both ice dynamics response¹¹ and subglacial water discharge¹².

Despite far-reaching implications, knowledge of the ice thickness distributions of the world's glaciers is remarkably limited. The Glacier Thickness Database (GlaThiDa), which centralizes ice thickness measurements outside the two ice sheets, presently contains information for only about 1,000 out of the 215,000 glaciers worldwide¹³. This is despite important advances in the instrumentation used to measure ice thickness^{14,15}, with airborne platforms now capable of operating in mountainous environments as well¹⁶.

Owing to the lack of direct measurements, relations between glacier area and ice volume¹⁷ have traditionally been used to estimate global glacier volumes^{18–21}. For individual glaciers, instead, a suite of methods that infer the spatial ice thickness distribution from surface characteristics have been proposed^{22–27}. Such methods use topographical information—typically extracted from digital elevation models (DEMs)—to estimate the distribution of the glacier's surface mass balance and, hence, its mass turnover.

The latter is then inverted for ice thickness by using principles of ice flow dynamics. Regional-scale estimates based on such methods have been presented^{7,28,29}, but only one estimate exists at the global scale³⁰. This seems unfortunate in light of the results of the recent ice thickness models intercomparison experiment (ITMIX)³¹, which showed how individual models can suffer from substantial uncertainties, and that pooling the results from different models significantly increases the estimate's robustness and accuracy.

Here we take advantage of the ITMIX findings and use a combination of up to five ice thickness estimation models^{29,30,32–34} (Fig. 1) to provide an ensemble-based estimate for the ice thickness distribution of each of the about 215,000 glaciers included in the Randolph Glacier Inventory (RGI) version 6.0 (ref. ³⁵). All the models use the glacier's surface topography, obtained from different DEM sources, and principles of ice flow dynamics to invert for local ice thickness (Methods and Supplementary Section 1). Model performance is assessed against observations in a cross-validation scheme (Methods and Supplementary Fig. 1), and inverse variance and bias weighting (Methods and Supplementary Table 1) are used to produce a consensus composite result. Subtraction of the so-obtained ice thickness distribution from the surface provides a corresponding bedrock topography.

Distribution of global ice volume

The regional distribution of the global glacier ice volume, which includes the share located below present sea level, is given in Fig. 2. Based on the composite solution, we estimate a global glacier volume of $158 \pm 41 \times 10^3 \text{ km}^3$ (Table 1). This corresponds to a potential sea level contribution of $0.32 \pm 0.08 \text{ m}$ when the volume already

¹Laboratory of Hydraulics, Hydrology and Glaciology (VAW), ETH Zurich, Zurich, Switzerland. ²Swiss Federal Institute for Forest, Snow and Landscape Research (WSL), Birmensdorf, Switzerland. ³Department of Geosciences, University of Fribourg, Fribourg, Switzerland. ⁴Institute of Geography, Friedrich-Alexander-University Erlangen-Nuremberg (FAU), Erlangen, Germany. ⁵Department of Geography, University of Zurich, Zurich, Switzerland. ⁶Institute of Atmospheric and Cryospheric Sciences, University of Innsbruck, Innsbruck, Austria. ⁷Interdisciplinary Programme in Climate Studies, Indian Institute of Technology Bombay, Mumbai, India. ⁸Hydro-Remote Sensing Applications (H-RSA) Group, Department of Civil Engineering, Indian Institute of Technology Bombay, Mumbai, India. *e-mail: daniel.farinotti@ethz.ch

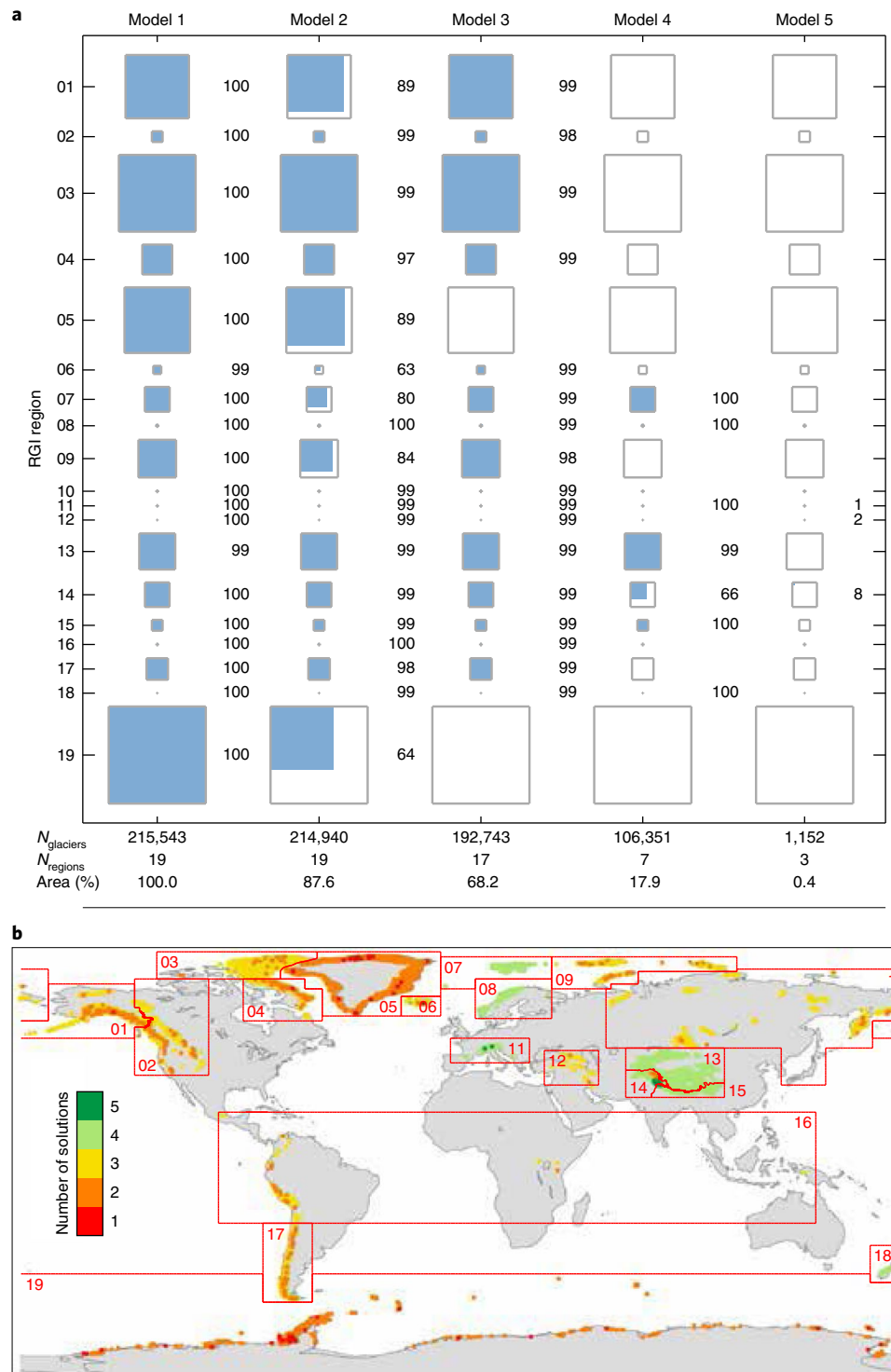


Fig. 1 | Overview of individual model contributions. **a**, Total glacier area (squares) for every RGI region (panel **b** and Table 1 give the region keys), together with the area portion (%) considered by each model (blue). For each model, the total number of considered glaciers (*N*_{glaciers}) and regions (*N*_{regions}) is provided, together with the share of total area (%) considered. **b**, Number of model solutions available for every glacier. Model 1, Huss and Farinotti³⁰; Model 2, Frey et al.²⁹; Model 3, Maussion et al.³³; Model 4, Fürst et al.³²; Model 5, Ramsankaran et al.³⁴.

located below sea level at present ($23.9 \pm 6.2 \times 10^3 \text{ km}^3$, or about 15% of the total) is subtracted. The largest glacier volumes are found in the Arctic ($74.7 \pm 19.4 \times 10^3 \text{ km}^3$ (47.3% of the global volume) when combining the Canadian and Russian Arctic, Greenland's periphery and Svalbard) and in the Antarctic periphery ($46.5 \pm 12.1 \times 10^3 \text{ km}^3$

(29.4%)). After Alaska ($19.0 \pm 4.9 \times 10^3 \text{ km}^3$ (12.0%)), High Mountain Asia—which consists of South and Central Asia—is the area with the largest ice volume ($7.0 \pm 1.8 \times 10^3 \text{ km}^3$ (4.4%)) outside the polar regions. Combined, the remaining nine regions only contain about 6.9% ($11.0 \pm 2.8 \times 10^3 \text{ km}^3$) of the global ice volume.

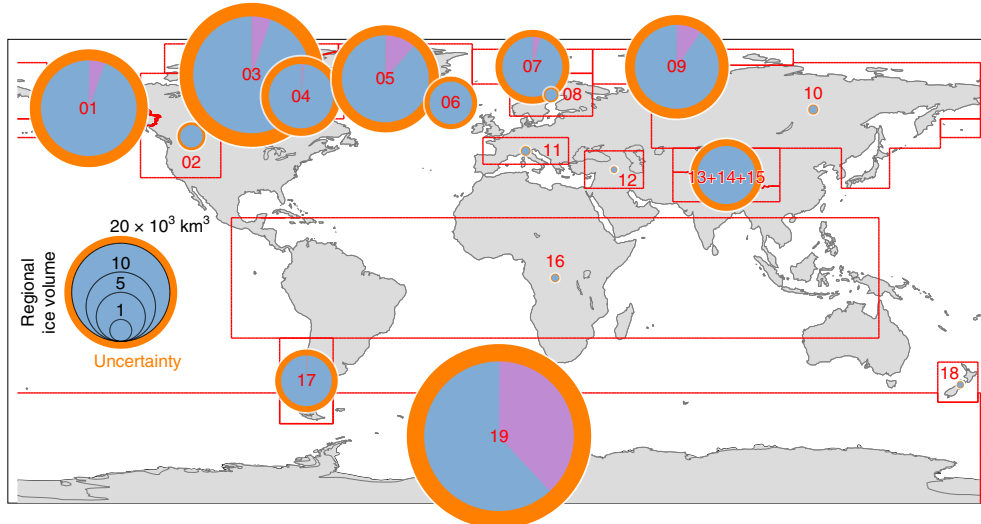


Fig. 2 | Regional distribution of the calculated glacier ice volume. The pie charts are centred over the considered RGI region (red labels and lines). The pie area is proportional to the calculated ice volume (Table 1) and discerns between the ice above (blue) and below (violet) present-day sea level. The outer ring (orange) reflects the estimated uncertainty (Methods).

Table 1 | Regionally aggregated summary statistics for the provided results

RGI region	N	A (km^2)	V (10^3 km^3)	\bar{h} (m)	SLE (mm)	BSL (%)
01 Alaska	27,108	86,677	18.98 ± 4.92	218	43.3 ± 11.2	5.4
02 Western Canada and United States	18,862	14,629	1.06 ± 0.27	72	2.6 ± 0.7	0.0
03 Arctic Canada North	4,549	104,920	28.33 ± 7.35	270	64.8 ± 16.8	5.3
04 Arctic Canada South	7,422	40,860	8.61 ± 2.23	210	20.5 ± 5.3	1.3
05 Greenland periphery	19,306	89,651	15.69 ± 4.07	175	33.6 ± 8.7	11.3
06 Iceland	567	11,052	3.77 ± 0.98	341	9.1 ± 2.4	0.2
07 Svalbard	1,615	33,932	7.47 ± 1.94	220	17.3 ± 4.5	4.1
08 Scandinavia	3,417	2,947	0.30 ± 0.08	101	0.7 ± 0.2	0.0
09 Russian Arctic	1,069	51,551	14.64 ± 3.80	283	32.0 ± 8.3	9.5
10 North Asia	5,144	2,399	0.14 ± 0.04	56	0.3 ± 0.1	0.0
11 Central Europe	3,927	2,091	0.13 ± 0.03	61	0.3 ± 0.1	0.0
12 Caucasus and Middle East	1,887	1,305	0.06 ± 0.02	48	0.2 ± 0.0	0.0
13 Central Asia	54,429	49,295	3.27 ± 0.85	66	7.9 ± 2.0	0.0
14 South Asia West	27,986	33,561	2.87 ± 0.74	85	6.9 ± 1.8	0.0
15 South Asia East	13,119	14,734	0.88 ± 0.23	59	2.1 ± 0.5	0.0
16 Low latitudes	2,940	2,341	0.10 ± 0.03	42	0.2 ± 0.1	0.0
17 Southern Andes	15,908	29,368	5.34 ± 1.39	181	12.8 ± 3.3	0.7
18 New Zealand	3,537	1,161	0.07 ± 0.02	63	0.2 ± 0.0	0.0
19 Antarctic and subantarctic ^a	2,751	132,771	46.47 ± 12.06	349	69.4 ± 18.0	38.1
Total	215,543	705,253	158.17 ± 41.03	224	324.3 ± 84.1	15.1

^aAs the Antarctic ice sheet is not included in this region, we refer to it as the Antarctic periphery throughout the manuscript. The number of considered glaciers (N) and their area (A) is given together with the regional glacier volume (V) and the corresponding average ice thickness (\bar{h}). The potential sea-level equivalent (SLE) accounts for the ice portion presently located below sea level (BSL). All numbers refer to the composite solution.

Significant ice volumes located below the present sea level, which would not contribute to future sea-level rise even if melted, are found in the Antarctic periphery (38% of the regional volume), Greenland periphery (11%), Russian Arctic (9.5%), Alaska (5.4%), and northern Arctic Canada (5.3%). In all cases, the relatively large percentages are indicative for the deeply incised fjord systems that characterize ocean-terminating glaciers in the polar regions³⁶.

Our estimate of the global glacier volume is about 18% lower than the average of previous estimates (Supplementary Table 2), but

relatively close (difference of -7.1%) to that reported by Huss and Farinotti³⁰. The latter study—referred to as HF12 in the following—is the only one to provide global-scale estimates for the ice thickness distribution of individual glaciers so far. Although our total ice volume agrees with that of HF12, the regional distributions differ substantially (Fig. 3). The most important difference is found in the Antarctic periphery, where our estimate is 24% higher, and is now close to the average of previous studies (Supplementary Table 2). The higher estimate is compensated by reduced ice volumes

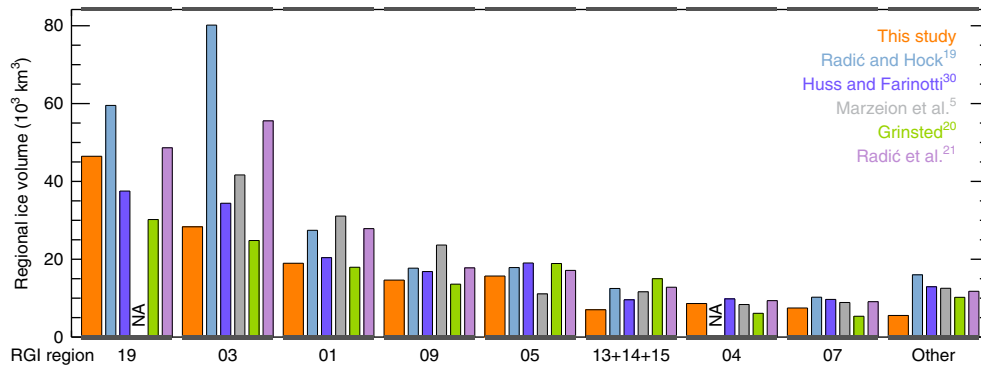


Fig. 3 | Overview of individual model contributions. NA indicates that a corresponding estimate was not available. Region labels follow those in Fig. 1 and Table 1.

obtained for the Arctic (-17% compared to HF12), High Mountain Asia (-27%) and other regions, specifically including the Southern Andes (-20%). When compared to the average of previous studies, the most striking difference is found for High Mountain Asia, where our results indicate a 46% lower total ice volume (Supplementary Table 2). The fraction of global ice volume located below present-day sea level is very close (within $\pm 2.5\%$) to a previous estimate³⁷ that was based on order-of-magnitude considerations.

Implications for glacier evolution, and ice discharge

The implications of the revised estimates, and the potential insights they provide, are demonstrated for the two regions in which the estimated total glacier volume has changed the most in comparison to HF12: High Mountain Asia and the Antarctic periphery.

For High Mountain Asia, we used the Global Glacier Evolution Model (GloGEM)¹⁰ to provide projections for the glacier evolution until 2100 (Methods). Keeping the model forcing and parameters unaltered but adjusting the initial ice thickness distribution of the simulations causes significant differences in the evolution of both the glacierized area and expected glacier runoff. Simulations performed by using the HF12 ice thickness (Simulation 1), for example, suggest that the region's glacier area (roughly $97,000\text{ km}^2$ according to the RGI) is likely to have shrunk by 50% by the late 2070s. Replacing the initial ice thickness distribution of the about 96,000 glaciers in the region with the here-presented results and repeating the simulations (Simulation 2) moves this point in time forward to the mid 2060s (Supplementary Fig. 2). The effect of a changed initial ice thickness distribution is noticeable in the projected future glacier water discharge as well (Supplementary Fig. 3). Simulation 1, for example, indicates that the average July–August runoff from the presently glacierized surfaces across High Mountain Asia could be reduced by roughly 15% by the 2090s when compared to present levels. In Simulation 2, this figure changes to a reduction by 24% , which corresponds to an additional July–August runoff decrease of $6 \times 10^9 \text{ m}^3 \text{ month}^{-1}$. In light of the importance of glacier melt for the regional water supply^{3,8,38}, these differences are unsettling, and call for a better characterization of the regional glacier ice volume. At the moment, the latter is hampered by the paucity of available in situ measurements, and is reflected in the large spread between results provided by individual models (Supplementary Fig. 4).

For the Antarctic periphery, we calculated the amount of ice discharged across the calving front of all ocean-terminating glaciers contained in the RGI. We did so by intersecting our distributed ice thickness estimates with observed ice flow velocities (Methods). The resulting total ice flux is $43 \pm 8 \text{ Gt a}^{-1}$, equivalent to about 3% of the calving flux from the entire Antarctic ice sheet³⁹. This quantity is of relevance because the non-floating portion of the discharged ice directly contributes to sea-level change. The subglacial topography

of glaciers in the Antarctic periphery is also of interest in light of the highly dynamic response observed for outlet glaciers after the loss of floating tongues and ice shelves⁴⁰. This response, which can result in a manifold acceleration in ice flow velocities⁴⁰, is recognized to be decisively modulated by the buttressing induced by local topography, including subglacial features⁴¹. Despite still being affected by considerable uncertainties (see the next section), the here-presented ice thickness estimates provide a better basis on which such dynamic responses can be estimated.

Causes of discrepancies, uncertainties and way forward

We attribute a large part of the differences with respect to HF12 to the way that individual glaciers are represented in the inventory that is at the base of our analysis. On the one hand, the quality and completeness of RGI version 6.0 has substantially improved compared to that of version 2.0, which was used in the earlier study. On the other hand, many glacier complexes are separated into individual units in the new inventory³⁵. These differences are best reflected in the reported total number of glaciers and area, with roughly 44,500 additional entries (+26%) in version 6.0 compared to version 2.0 despite a minor change (-4%) in the total area. Although the addition of formerly disregarded, mostly small, glaciers is unlikely to affect the estimated regional volumes significantly, the failure to separate glacier complexes is known to introduce biases towards higher ice thicknesses, because a clear relation exists between glacier area and volume. We suggest that the above changes (Supplementary Fig. 5 gives an illustrative example) particularly affected the estimates for High Mountain Asia, with the newer inventory discerning almost 30,000 additional glaciers (+44%) but reporting a 19% smaller total area. For that region, our total volume estimate now lies even below the lowest one reported in Frey et al.²⁹.

For the Antarctic periphery, we attribute the large differences with respect to HF12 to the DEMs used to represent the glacier surfaces (Methods). Although HF12 exclusively used data from the Advanced Spaceborne Thermal Emission and Reflection Radiometer (ASTER) DEM⁴² (known to be noisy for some parts of the Antarctic), here we use data from the much-improved Radarsat Antarctic Mapping Project (RAMP⁴³). The smoother surfaces of the latter product cause local surface slopes to be smaller, which in turn results in larger ice thicknesses due to the inverse relation to ice flow driving stress³¹.

The significant differences between regional estimates provided by various studies (Fig. 3) and models (Supplementary Fig. 4) is a clear indication that the present estimates still suffer from significant uncertainties. Two main sources can be discerned in this respect: the uncertainty in the models used to estimate the ice thickness, and the uncertainty in the driving input data. Although the first uncertainty can be reasonably quantified (Methods) and can be

reduced by combining the results of different approaches³¹, ample room for model improvement still exists. This is particularly evident when considering point-by-point comparisons between measured and modelled ice thicknesses: although the mean thickness is usually well captured (Supplementary Fig. 1) and no bias with respect to glacier size can be discerned (Supplementary Fig. 2), all the models regularly show local deviations of up to twice the observed mean ice thickness. This is not least related to the ill-posed nature of the ice-thickness-inversion problem. As outlined by Bahr et al.⁴⁴, inverting the surface characteristics for ice thickness can create a calculation instability that grows exponentially with glacier size, and random errors from this instability can overwhelm other sources of uncertainty. Although (1) our ensemble approach minimizes the influence of random errors and (2) the ill-posed nature of the problem is taken into account through spatial smoothing of individual model outputs, such limitations have to be kept in mind when using the results for analyses that are potentially sensitive to small-scale topography.

Ways to further improve the model performance—which include the assimilation of additional surface information such as ice flow velocities, anticipated to soon become available at the global scale—have been sketched previously³¹. To improve the consistency and completeness of global data sets for glacier outlines, surface elevation models and measured ice thickness would, however, be of equal importance to further improve the reliability of regional-scale estimates. Individual, dedicated campaigns in particularly data-scarce regions could prove efficient towards this target, provided that the results are made openly available.

For the time being, the results presented here provide a consensus estimate of the ice thickness distribution of all the glaciers on Earth outside the polar ice sheets. The results are anticipated to have implications ranging from projected sea-level change rates to estimated future water availability. The results can be retrieved from <https://doi.org/10.3929/ethz-b-000315707>.

Online content

Any methods, additional references, Nature Research reporting summaries, source data, statements of data availability and associated accession codes are available at <https://doi.org/10.1038/s41561-019-0300-3>.

Received: 21 August 2018; Accepted: 2 January 2019;

Published online: 11 February 2019

References

- Vaughan, D. et al. in *Climate Change 2013: The Physical Science Basis* (eds Stocker, T. F. et al.) 317–382 (IPCC, Cambridge Univ. Press, 2013).
- Lambeck, K., Rouby, H., Purcell, A., Sun, Y. & Sambridge, M. Sea level and global ice volumes from the Last Glacial Maximum to the Holocene. *Proc. Natl Acad. Sci. USA* **111**, 15296–15303 (2014).
- Kaser, G., Großhauser, M. & Marzeion, B. Contribution potential of glaciers to water availability in different climate regimes. *Proc. Natl Acad. Sci. USA* **107**, 20223–20227 (2010).
- Rodell, M. et al. Emerging trends in global freshwater availability. *Nature* **557**, 651–659 (2018).
- Marzeion, B., Jarosch, A. & Hofer, M. Past and future sea-level change from the surface mass balance of glaciers. *Cryosphere* **6**, 1295–1322 (2012).
- Church, J. et al. in *Climate Change 2013: The Physical Science Basis* (eds Stocker, T. F. et al.) 1137–1216 (IPCC, Cambridge Univ. Press, 2013).
- Kraaijenbrink, P., Lutz, A., Bierkens, M. & Immerzeel, W. Impact of a 1.5°C global temperature rise on the glaciers of High Mountain Asia. *Nature* **549**, 257–260 (2017).
- Huss, M. & Hock, R. Global-scale hydrological response to future glacier mass loss. *Nat. Clim. Change* **8**, 135–140 (2018).
- Gabbie, J., Farinotti, D., Bauder, A. & Maurer, H. Ice volume distribution and implications on runoff projections in a glacierized catchment. *Hydrol. Earth Syst. Sci.* **16**, 4543–4556 (2012).
- Huss, M. & Hock, R. A new model for global glacier change and sea-level rise. *Front. Earth Sci.* **3**, 54 (2015).
- Nias, I., Cornford, S. & Payne, A. New mass conserving bedrock topography for Pine Island Glacier impacts simulated decadal rates of mass loss. *Geophys. Res. Lett.* **45**, 3173–3181 (2018).
- Amundson, J. & Carroll, D. Effect of topography on subglacial discharge and submarine melting during tidewater glacier retreat. *J. Geophys. Res. Earth Surf.* **123**, 66–79 (2017).
- Gärtner-Roer, I. et al. *Glacier Thickness Database 2.0* (World Glacier Monitoring Service, 2016); <https://doi.org/10.5904/wgms-glathida-2016-07>
- Allen, C. *IceBridge MCORDS L2 Ice Thickness* (NASA DAAC at the National Snow and Ice Data Center, 2010).
- Zamora, R., Uribe, J., Oberreuter, J. & Rivera, A. Ice thickness surveys of the southern Patagonian ice field using a low frequency ice penetrating radar system. In *First IEEE Inter. Symp. Geosci. Remote Sensing (GRSS-CHILE)* 1–4 (IEEE, 2017).
- Rutishauser, A., Maurer, H. & Bauder, A. Helicopter-borne ground-penetrating radar investigations on temperate alpine glaciers: a comparison of different systems and their abilities for bedrock mapping. *Geophysics* **81**, WA119 (2016).
- Bahr, D. B., Pfeffer, W. T. & Kaser, G. A review of volume-area scaling of glaciers. *Rev. Geophys.* **53**, 95–140 (2015).
- Dyurgerov, M. & Meier, M. *Glaciers and the Changing Earth System: A 2004 Snapshot* Institute of Arctic and Alpine Research Occasional Paper 58 (Univ. Colorado, 2005).
- Radić, V. & Hock, R. Regional and global volumes of glaciers derived from statistical upscaling of glacier inventory data. *J. Geophys. Res.* **115**, F01010 (2010).
- Grinsted, A. An estimate of global glacier volume. *Cryosphere* **7**, 141–151 (2013).
- Radić, V. et al. Regional and global projections of twenty-first century glacier mass changes in response to climate scenarios from global climate models. *Clim. Dyn.* **42**, 37–58 (2014).
- Farinotti, D., Huss, M., Bauder, A., Funk, M. & Truffer, M. A method to estimate ice volume and ice thickness distribution of alpine glaciers. *J. Glaciol.* **55**, 422–430 (2009).
- Morlighem, M. et al. A mass conservation approach for mapping glacier ice thickness. *Geophys. Res. Lett.* **38**, L19503 (2011).
- Linsbauer, A., Paul, F. & Haeberli, W. Modeling glacier thickness distribution and bed topography over entire mountain ranges with GlabTop: application of a fast and robust approach. *J. Geophys. Res.* **117**, F03007 (2012).
- McNabb, R. et al. Using surface velocities to calculate ice thickness and bed topography: a case study at Columbia Glacier, Alaska. *J. Glaciol.* **58**, 1151–1164 (2012).
- van Pelt, W. J. J. et al. An iterative inverse method to estimate basal topography and initialize ice flow models. *Cryosphere* **7**, 987–1006 (2013).
- Brinkerhoff, D. J., Aschwanden, A. & Truffer, M. Bayesian inference of subglacial topography using mass conservation. *Front. Earth Sci.* **4**, 1–15 (2016).
- Clarke, G. K. C. et al. Ice volume and subglacial topography for western Canadian glaciers from mass balance fields, thinning rates, and a bed stress model. *J. Clim.* **26**, 4282–4430 (2013).
- Frey, H. et al. Estimating the volume of glaciers in the Himalayan–Karakoram region using different methods. *Cryosphere* **8**, 2313–2333 (2014).
- Huss, M. & Farinotti, D. Distributed ice thickness and volume of all glaciers around the globe. *J. Geophys. Res.* **117**, F04010 (2012).
- Farinotti, D. et al. How accurate are estimates of glacier ice thickness? Results from ITMIX, the Ice Thickness Models Intercomparison eXperiment. *Cryosphere* **11**, 949–970 (2017).
- Fürst, J. J. et al. Application of a two-step approach for mapping ice thickness to various glacier types on Svalbard. *Cryosphere* **11**, 2003–2032 (2017).
- Maussion, F. et al. The Open Global Glacier Model (OGGM)v1.0. *Geosci. Model Develop. Discuss.* **2018**, 1–33 (2018).
- Ramsankaran, R., Pandit, A. & Azam, M. Spatially distributed ice-thickness modelling for Chhota Shigri Glacier in western Himalayas, India. *Int. J. Remote. Sens.* **39**, 3320–3343 (2018).
- RGI Consortium *Randolph Glacier Inventory—A Dataset of Global Glacier Outlines: Version 6.0* (Global Land Ice Measurements from Space (GLIMS), 2017).
- Herman, F., Beaud, F., Champagnac, J.-D., Lemieux, J.-M. & Sternai, P. Glacial hydrology and erosion patterns: a mechanism for carving glacial valleys. *Earth Planet. Sci. Lett.* **310**, 498–508 (2011).
- Haeberli, W. & Linsbauer, A. Global glacier volumes and sea level—small but systematic effects of ice below the surface of the ocean and of new local lakes on land. *Cryosphere* **7**, 817–821 (2013).
- Immerzeel, W. W. & Bierkens, M. F. P. Asia's water balance. *Nat. Geosci.* **5**, 841–842 (2012).
- Depoorter, M. A. et al. Calving fluxes and basal melt rates of Antarctic ice shelves. *Nature* **502**, 89–92 (2013).
- Rignot, E. et al. Accelerated ice discharge from the Antarctic Peninsula following the collapse of Larsen B ice shelf. *Geophys. Res. Lett.* **31**, L18401 (2004).

41. Fürst, J. et al. The safety band of Antarctic ice shelves. *Nat. Clim. Change* **6**, 479–482 (2016).
42. Tachikawa, T., Hato, M., Kaku, M. & Iwasaki, A. Characteristics of ASTER GDEM version 2. In *Proc. IEEE Int. Geosci. Remote Sensing Symp. (IGARSS) 2011* 3657–3660 (IEEE, 2011).
43. Liu, H., Jezek, K., Li, B. & Zhao, Z. *Radarsat Antarctic Mapping Project Digital Elevation Model, Version 2* (NASA National Snow and Ice Data Center Distributed Active Archive Center, 2015).
44. Bahr, D. B., Pfeffer, W. T. & Kaser, G. Glacier volume estimation as an ill-posed inversion. *J. Glaciol.* **60**, 922934 (2014).

Acknowledgements

The contribution from J.J.F. was supported by the German Research Foundation (DFG grant no. FU1032/1-1), with numerical simulations facilitated by the high-performance computing centre at the University of Erlangen-Nuremberg (Regionales Rechenzentrum Erlangen (RRZE)). The support from R. Ramsankaran's research team at the Indian Institute of Technology Bombay is acknowledged. We thank the International Association of Cryospheric Sciences (IACS), co-chairs L. M. Andreassen and H. Li, and the members of the IACS Working Group on Glacier Ice Thickness Estimation for the support during the work. The analyses were performed in the frame of the Working Group's Global Glacier Thickness Initiative (G2TI).

Author contributions

D.F. conceived the study, performed the analyses of the results and drafted the manuscript, to which all the authors contributed. M.H., J.L. and D.F. prepared the necessary input data. M.H., J.J.F., H.M., F.M. and A.P. performed the calculations with individual models. M.H. and D.F. performed the GloGEM and Antarctic ice-discharge calculations, respectively.

Competing interests

The authors declare no competing interests.

Additional information

Supplementary information is available for this paper at <https://doi.org/10.1038/s41561-019-0300-3>.

Reprints and permissions information is available at www.nature.com/reprints.

Correspondence and requests for materials should be addressed to D.F.

Publisher's note: Springer Nature remains neutral with regard to jurisdictional claims in published maps and institutional affiliations.

© The Author(s), under exclusive licence to Springer Nature Limited 2019

Methods

Glacier morphology and measured ice thickness. All ice thickness estimates refer to the outlines provided through the RGI version 6.0 (ref. ³⁵). For every glacier (215,547 entities in total), the surface topography was extracted from either the hole-filled Shuttle Radar Topography Mission (SRTM) DEM version 4 (latitudes between 60°N and 60°S (ref. ⁴⁵)), the ASTER Global DEM version 2 (ref. ⁴²) and the RAMP DEM version 2 (ref. ⁴⁶) (south of 60°S), or the Arctic DEM version 2.0 (north of 60°N (ref. ⁴⁷)). Regions affected by data voids in the Arctic DEM were replaced by DEM3 (ref. ⁴⁸). To reduce the computational demand and depending on glacier size, the DEMs were resampled to a resolution of 25, 50, 100 or 200 m. The measured ice thickness was obtained from the GlaThiDa version 2.0 (ref. ¹³), which provides ice thickness information for 1,085 glaciers.

Ice thickness estimates. The ice thickness of individual glaciers was estimated by using the above information and up to five different models. Ordered by the glacier area for which a solution was provided (Fig. 1), the models included those by Huss and Farinotti³⁰ (Model 1), Frey et al.²⁹ (Model 2), Maussion et al.³³ (Model 3), Fürst et al.³² (Model 4) and Ramsankaran et al.³⁴ (Model 5). These models are capable of inverting for glacier ice thickness distributions at the mountain range scale. All the models infer the ice thickness distribution from surface characteristics (such as elevation and slope), an estimate of the glacier mass turnover and principles of ice flow dynamics. A summary description of the five models is given in Farinotti et al.³¹, and Supplementary Section 1 and the original publications provide the details. For the ice thickness distribution of Svalbard, the area covered by the recent estimate of Fürst et al.⁴⁹ is replaced with that estimate. The remaining area is treated in the same way as the other regions. Fürst et al.⁴⁹ is based on Model 4, but used an additional set of more than 900,000 in situ ice thickness measurements that are not yet included in GlaThiDa. This provided substantially better model constraints than available within this study. Supplementary Figs. 6–24 provide examples for the ice thickness distribution generated by the individual models for selected glaciers (one per RGI region). Note that not all of the models provided an estimate for all of the RGI entries (Fig. 1), mainly because the requirements for manual interactions or the computational cost were unaffordable for the global-scale application.

Model weighting and uncertainty estimates. The final results are based on a composite solution $\hat{\mu}$ derived on a glacier-by-glacier basis through inverse variance and bias weighting⁵⁰. For any given location, and assuming independence between the local ice thickness estimates h_i provided by the $n \leq 5$ models, $\hat{\mu}$ is computed as:

$$\hat{\mu} = \frac{\sum h_i w_i^{-1}}{\sum w_i^{-1}} \quad (1)$$

where $w_i = |b_i| + \sigma_i^2$ is a weighting that reflects both the bias b_i and the variance σ_i^2 of the result produced by model i ($|b_i|$ denotes the absolute value of b_i and ensures that both over- and underestimates are penalized). To estimate b_i and σ_i^2 , a cross-validation experiment was performed in which one-third of the available ice thickness measurements was randomly selected and used for model calibration, with the remaining two-thirds used for model validation. The experiment was repeated three times, and the deviations between modelled and measured ice thicknesses were expressed relatively to the mean ice thickness \bar{h} . The so-obtained deviations were pooled across the three experiments, and the mean and interquartile range of the pool were taken as an estimate for b_i / \bar{h}_i and $1.5\sigma_i / \bar{h}_i$, respectively. The results of the cross validation are shown in Supplementary Fig. 1 and yielded relative weights of 22%, 19%, 18%, 28% and 13% for Models 1–5, respectively (last row of Supplementary Table 1). With the above notation, the variance of $\hat{\mu}$ is given by:

$$\sigma_{\hat{\mu}}^2 = \frac{1}{\sum \sigma_i^{-2}} \quad (2)$$

which is the basis for the presented accuracy estimates. Although we assume independence between the results obtained for a given glacier from different models, the results for different glaciers are assumed to be strongly correlated when they originate from the same model (or from the composite solution). When calculating regional totals, the uncertainties estimated for individual glaciers are thus summed. To assess the sensitivity of the above weighting strategy, regionally differentiated weights were tested as well. In that case, the weights in equation (1) were calculated by pooling the results of the cross-validation experiment separately for every RGI region (upper part of Supplementary Table 1). The results are insensitive (differences below 1%) to this alternative weighting scheme (Supplementary Table 3).

Sea-level change equivalents. The conversion between total glacier ice volume V_{tot} and potential sea-level change h_{SLE} was performed by (1) assuming a

bulk ice density of $\rho_{\text{ice}} = 900 \text{ kg m}^{-3}$, an ocean area of $A_{\text{ocean}} = 3.625 \times 10^8 \text{ km}^2$ and a mean ocean density of $\rho_{\text{ocean}} = 1,028 \text{ kg m}^{-3}$ (ref. ⁵¹), (2) neglecting the steric and isostatic effects and (3) subtracting glacier volumes V_{BSL} presently located below sea level:

$$h_{\text{SLE}} = \frac{V_{\text{tot}} - V_{\text{BSL}}}{A_{\text{ocean}}} \frac{\rho_{\text{ice}}}{\rho_{\text{ocean}}} \quad (3)$$

Future projections for High Mountain Asia. Reconstruction for the past (1998–2016) and projections for the future (2017–2100) glacier evolution and corresponding glacier runoff were obtained by forcing the GloGEM¹⁰ with climate reanalysis data⁵² and outputs from 14 different global climate models⁵³ driven by Representative Concentration Pathway 4.5 (a midrange scenario for future climate evolution⁵⁴), respectively. The model calibration, parameter choice and downscaling of climate model outputs are identical to those in Huss and Hock¹⁰. Two different simulations were performed for the time period 1998–2100, the only difference being the ice thickness distribution used to initialize the model. The model provides the glacier area (with an annual time step) and glacier runoff (with a monthly time step) of every glacier individually, and the results are aggregated over RGI regions 13, 14 and 15 (Table 1 and Fig. 2). Uncertainties due to unknown future climate evolution are taken into account through the output of different climate models. Further uncertainties are not accounted for explicitly as they have been shown to be comparatively small¹⁰.

Ice discharge from Antarctic glaciers. Ice discharge estimates for glaciers in the Antarctic periphery are based on surface ice flow velocities provided in Rignot et al.⁵⁵. For every glacier, the calving front was identified by selecting portions of the glacier outline that have a bedrock located below present-day sea level (roughly 250 of the 2,751 glaciers in the region are detected to have such a calving front). The volumetric ice discharge was then obtained by multiplying the local, depth-averaged ice flow velocity with the local ice thickness and by integrating the so-obtained values over the calving front length. Uncertainties in surface velocities are provided within the data set⁵⁵, whereas uncertainties in depth-averaged values are estimated by considering two end members: the first assumes that the entire surface motion is due to basal sliding (plug flow), and the second assumes the surface velocity is entirely due to ice deformation. The reported results refer to the average of the two end members. A bulk density of 900 kg m^{-3} was used to convert ice volume flux to mass flux.

Code availability

The codes used to generate individual results are available through the contact information from the original publications. Requests for further materials should be directed to D.F.

Data availability

The ice thickness distribution of all about 215,000 glaciers, as estimated with the individual models and the composite solution, is available at <https://doi.org/10.3929/ethz-b-000315707>.

References

45. Jarvis, J., Reuter, H., Nelson, A. & Guevara, E. *Hole-Filled SRTM for the Globe Version 4* (CGIAR Consortium for Spatial Information, 2008).
46. Liu, S. et al. Glacier retreat as a result of climate warming and increased precipitation in the Tarim river basin, northwest China. *Ann. Glaciol.* **43**, 91–96 (2006).
47. Porter, C. et al. ArcticDEM V1 (Harvard Dataverse, 2017); <https://doi.org/10.7910/DVN/OHUKH>
48. de Ferranti, J. *A Worldwide 3 Arc Seconds DEM* (2014); <http://viewfinderpanoramas.org/dem3.html>
49. Fürst, J. et al. The ice-free topography of Svalbard. *Geophys. Res. Lett.* **45**, 760–711 (2018).
50. Hartung, J., Knapp, G. & Sinha, B. *Statistical Meta-analysis with Applications* (John Wiley & Sons, Hoboken, 2008).
51. Conkright, M. et al. *World Ocean Atlas 2001: Objective Analyses, Data Statistics, and Figures*, CD-ROM Documentation 17 (National Oceanographic Data Center, Silver Spring, 2002).
52. Dee, D. et al. The ERA-Interim reanalysis: configuration and performance of the data assimilation system. *Q. J. R. Meteorol. Soc.* **137**, 553–597 (2011).
53. Taylor, K., Stouffer, R. & Meehl, G. An overview of CMIP5 and the experiment design. *Bull. Am. Meteorol. Soc.* **93**, 485–498 (2012).
54. Meinshausen, M. et al. The RCP greenhouse gas concentrations and their extensions from 1765 to 2300. *Climatic Change* **109**, 213–241 (2011).
55. Rignot, E., Mouginot, J. & Scheuchl, B. *MEaSUREs InSAR-Based Antarctica Ice Velocity Map, Version 2* (NASA National Snow and Ice Data Center Distributed Active Archive Center, 2017).

In the format provided by the authors and unedited.

A consensus estimate for the ice thickness distribution of all glaciers on Earth

Daniel Farinotti^{1,2*}, Matthias Huss^{1,3}, Johannes J. Fürst⁴, Johannes Landmann^{1,2}, Horst Machguth^{3,5}, Fabien Maussion^{1,6} and Ankur Pandit^{7,8}

¹Laboratory of Hydraulics, Hydrology and Glaciology (VAW), ETH Zurich, Zurich, Switzerland. ²Swiss Federal Institute for Forest, Snow and Landscape Research (WSL), Birmensdorf, Switzerland. ³Department of Geosciences, University of Fribourg, Fribourg, Switzerland. ⁴Institute of Geography, Friedrich-Alexander-University Erlangen-Nuremberg (FAU), Erlangen, Germany. ⁵Department of Geography, University of Zurich, Zurich, Switzerland. ⁶Institute of Atmospheric and Cryospheric Sciences, University of Innsbruck, Innsbruck, Austria. ⁷Interdisciplinary Programme in Climate Studies, Indian Institute of Technology Bombay, Mumbai, India. ⁸Hydro-Remote Sensing Applications (H-RSA) Group, Department of Civil Engineering, Indian Institute of Technology Bombay, Mumbai, India. *e-mail: daniel.farinotti@ethz.ch

Supplementary Material

A consensus estimate for the ice thickness distribution of all glaciers on Earth

Daniel Farinotti^{1,2}, Matthias Huss^{1,3}, Johannes J. Fürst⁴, Johannes Landmann^{1,2}, Horst Machguth^{3,5}, Fabien Maussion⁶, and Ankur Pandit⁷

¹ Laboratory of Hydraulics, Hydrology and Glaciology (VAW), ETH Zurich, Zurich, Switzerland

² Swiss Federal Institute for Forest, Snow and Landscape Research (WSL), Birmensdorf, Switzerland

³ Department of Geosciences, University of Fribourg, Fribourg, Switzerland

⁴ Inst. of Geography, Friedrich-Alexander-University Erlangen-Nuremberg (FAU), Erlangen, Germany

⁵ Department of Geography, University of Zurich, Zurich, Switzerland

⁶ Institute of Atmospheric and Cryospheric Sciences, University of Innsbruck, Innsbruck, Austria

⁷ Interdisciplinary Programme in Climate Studies, Indian Institute of Technology, Bombay, India

¹ **S 1 Setup of individual models**

² The models used within the study have been presented in earlier publications (Huss and Farinotti,
³ 2012; Frey et al., 2014; Fürst et al., 2017; Ramsankaran et al., 2018; Maussion et al., 2018) and are
⁴ summarized in Farinotti et al. (2017). This section mainly provides additional implementation-
⁵ details used for the present work.

⁶ **S 1.1 Model 1 (*HF-model*) – Huss and Farinotti (2012)**

⁷ The *HF-model* by Huss and Farinotti (2012) is based on mass conservation and principles of
⁸ ice flow dynamics. Basically, the approach estimates the ice volume flux along the glacier, and
⁹ converts it into ice thickness by using Glen's flow law (Glen, 1955). Glacier hypsometry and
¹⁰ surface characteristics (mean slope and glacier width) are evaluated for 10 m elevation bands,
¹¹ and all calculations are performed with this simplified two dimensional shape. Apparent mass
¹² balance gradients for the ablation and accumulation area (Farinotti et al., 2009) are estimated
¹³ based on the continentality of the glacier. Ice volume fluxes along the glacier are converted
¹⁴ into ice thickness using an integrated form of Glen's flow law. Longitudinal variations in valley
¹⁵ shape and basal shear stress are taken into account. Simple parametrisations describe both the
¹⁶ temperature-dependence of the flow rate factor and the variability in basal sliding. Calculated
¹⁷ mean elevation-band thickness is extrapolated to each cell of a regular grid considering local
¹⁸ surface slope, and the distance from the glacier margin. For marine-terminating glaciers, a fixed
¹⁹ ice volume flux is prescribed at the glacier terminus.

²⁰ For the here presented results, the model was calibrated to the available ice thickness measure-
²¹ ments by optimizing parameters specific to each RGI region. No model tuning was performed
²² to reproduce ice thickness observations of individual glaciers. The misfit with observations was
²³ assessed by evaluating (i) the region-by-region average of the mean deviations of all points of
²⁴ individual glaciers, (ii) the glacier-area-weighted average of the mean deviation over all points
²⁵ of individual glaciers, (iii) the average of the difference between calculated and reported mean
²⁶ ice thickness, and (iv) the glacier-area-weighted average of the difference between calculated
²⁷ and reported mean ice thickness. Original model parameters used in Huss and Farinotti (2012)
²⁸ were adjusted to minimize each of the criteria (i) to (iv), with the aim of minimizing systematic
²⁹ deviations from the observations. For roughly half of the regions, no re-calibration was neces-
³⁰sary. For the remaining RGI regions, the apparent mass balance gradient \bar{db}/dz (see Equation 1
³¹ in Huss and Farinotti, 2012) was adjusted within physically reasonable bounds. For two RGI
³² regions, also the flow rate factor A_f (Equation 5 in Huss and Farinotti, 2012) was re-calibrated.

³³ **S 1.2 Model 2 (*GlabTop2*) – Frey et al. (2014)**

³⁴ The *GlabTop2* model is based on the same concepts as presented in Linsbauer et al. (2012),
³⁵ and uses an empirical relation between average basal shear stress and glacier elevation range
³⁶ (Haeberli and Hoelzle, 1995) to calculate the ice thickness at individual locations. The laborious
³⁷ process of manually drawing branchlines, required in the original approach (Linsbauer et al.,
³⁸ 2012), is avoided by determining the local surface slope from the average of all grid cells within
³⁹ a predefined elevation buffer. This makes the entirely grid-based method applicable to the large
⁴⁰ scale. In a first step, an ice thickness is calculated at a set of randomly selected cells. In a
⁴¹ second step, this thickness is interpolated to the entire glacier area. To achieve realistic glacier
⁴² cross-sections, the interpolation scheme assigns a minimum, non-zero ice thickness to all grid

43 cells directly adjacent to the glacier margin.
44 Parameter selection for the *GlabTop2* model was identical to the one described in Farinotti
45 et al. (2017), with the exception of the shape factor f (see Equation 3 in Frey et al., 2014).
46 For the latter, an empirically derived function of the form $f = a \cdot (n_g/n_m)^b$ was used, where
47 n_g is the total number of grid cells of a glacier, n_m is the number of glacier grid cells that are
48 directly adjacent to the glacier margin, and a and b are two empirical coefficients. The additional
49 constraint $f \leq 1$ was imposed. Coefficients of $a = 5596$ and $b = 0.1688$ were determined during
50 the cross-validation experiment (see Methods in the main article) by minimizing the difference
51 between (i) the average ice thickness given by the measurements and (ii) the average thickness
52 given by the model at the corresponding locations (no calibration at the level of individual points
53 was performed). Note that the dependency of f on $r = n_g/n_m$ can be interpreted as the effect
54 of the drag from valley walls on glacier flow (Paterson, 1994). For a given surface slope, a low
55 r value (typical for a valley-type glacier) results in a higher ice thickness than a high r value
56 (typical for ice caps). Values of f were limited to ≤ 1 , thus varying from 0.5596 to 1.
57 For the ice thickness calculations, DEMs with a spatial resolution below 75 m were resampled
58 to 75 m, and re-brought to the original resolution afterwards. This is to reduce the noise that
59 is introduced when strong, small-scale variations in surface slope occur (such variations directly
60 affect the calculated ice thickness through the dependence on surface slope; e.g. Frey et al.,
61 2014; Farinotti et al., 2017). No thickness calculations were performed when (1) the provided
62 surface DEM contained negative values for more than 5 % of the area, and (2) the estimated ice
63 thickness was unrealistically high. To discern case (1), an arbitrary threshold of 100 m below
64 sea level was used. If this threshold was reached by fewer than 5% of the DEM extent, the
65 corresponding elevations were set to sea level (0 m a.s.l.); if the threshold was reached by more
66 than 5% of the DEM extent, the glacier was not considered. To discern case (2), a threshold of
67 900 m ice thickness was set. In cases where the threshold was met by 20% or more of the glacier
68 domain, the results were discarded. The number of so-excluded glaciers is very small (0.05 % of
69 the total) but the glaciers represent a disproportionately large fraction of both the global glacier
70 area (ca. 12 %) and volume (ca. 28 %).

71 S 1.3 Model 3 (*OGGM*) – Maussion et al. (2018)

72 The *Open Global Glacier Model* (*OGGM*; Maussion et al., 2018) is an open-source model for
73 glacier dynamics applicable on any glacier in the world. The ice thickness inversion scheme relies
74 on a mass-conservation approach similar to that of Farinotti et al. (2009), but is fully automated.
75 The ice thickness is computed from mass turnover and the shallow ice approximation along
76 multiple flowlines computed with the algorithm of Kienholz et al. (2014). A major difference
77 from other models is that OGGM relies on gridded climate data (CRU in this instance; Harris
78 et al., 2014) to compute the mass turnover, and not on predefined linear gradients.
79 The OGGM parameter calibration for this study was limited to (i) the interpolation parameters
80 used to translate the flowline thickness to a distributed ice thickness map, and (ii) the creep
81 parameter A in Glen's flow law (Glen, 1955). All other parameters are kept to their default
82 values (see Maussion et al., 2018). The interpolation parameters were selected to minimize the
83 glacier-wide root mean square deviation from actual ice thickness measurements, with A chosen
84 to minimize the glacier-wide bias. Once the interpolation step was fixed, Glen's A was chosen
85 to minimize the bias to all point observations in a given cross-validation set.
86 Unlike other models, OGGM does not rely on any regional tuning, i.e. the same set of parameters
87 is used globally and for each cross-validation set. The reasoning behind this decision is that RGI
88 regions are often arbitrary, and do not necessarily represent an homogeneous entity in terms

89 of climate or glaciological processes. Regional tuning might thus introduce artificial, model-
90 dependant differences between regions that are not found in reality.

91 A subjective assessment of the main sources of uncertainty (not ordered by importance) are (1)
92 the reliance on actual gridded climate data to estimate the mass-turnover, (2) the interpolation
93 step required to transpose the flowline representation into a two dimensional one, (3) uncer-
94 tainties in the actual ice dynamics parameters (deformation and sliding in particular), and (4)
95 uncertainties in the location and detection of glacier ice-divides.

96 **S 1.4 Model 4 (no specific name so far)– Fürst et al. (2017)**

97 The approach by Fürst et al. (2017) is primarily based on mass conservation and solves for a
98 basin-wide thickness field. A detailed description and performance analysis for various glacier
99 types on Svalbard was presented in the mentioned publication. The approach is split into two
100 steps to ensure wide applicability. For the global application, only the first step was applicable
101 since no surface velocities were available. Similar as for Models 1 and 3, this step relies on the
102 shallow-ice approximation for a flux-thickness conversion. Point measurements of ice thickness
103 are readily assimilated and reproduced by an automatic viscosity calibration.

104 The only adaptation concerns the ability to use information on mean glacier thickness (provided
105 within the *Glacier Thickness Database*; WGMS, 2016). For this purpose, a glacier-wide uniform
106 ice viscosity is calibrated such that the mean glacier thickness is reproduced. Information
107 on surface mass balance (SMB) for each glacier is based on the results of the *Global Glacier
108 Evolution Model (GloGEM*; Huss and Hock, 2015). The flowline SMB is averaged for the period
109 1980–2010. Values are extrapolated over the drainage basin following elevation bands. For
110 marine terminating glaciers, surface elevation changes were set to zero. For land-terminating
111 glaciers, elevation changes are parametrized by an empirical relations given in Huss et al. (2010),
112 which distinguishes between three glacier area classes.

113 **S 1.5 Model 5 (*GlabTop2_IITB version*) – Ramsankaran et al. (2018)**

114 The *GlabTop2_IITB version* (referred to as *RAAglabtop2* in Farinotti et al., 2017) is an inde-
115 pendent implementation of the *GlabTop2* model developed by Frey et al. (2014) (Model 2 above;
116 cf. Sec. S 1.2).

117 Calibration of the model followed Ramsankaran et al. (2018). In a nutshell, the method’s
118 shape factor f (see Equation 3 in Ramsankaran et al., 2018) is used as the only calibration
119 parameter, and direct ice thickness observations are used to iteratively adjust f so that the
120 squared differences between modelled and observed ice thicknesses are minimized. Since no
121 direct ice thickness estimates were available for the vast majority of the 1152 glaciers considered
122 by the model, a set of 31 simulations were performed by varying f in the interval $f = [0.6, 0.9]$
123 with a spacing of 0.01. The so-obtained ice thickness distributions were then stacked by
124 averaging pixel-wise the local ice thickness obtained from the individual simulations. The so
125 obtained distribution was used as the best estimate.

Table S1: Weights assigned to individual models (M1 to M5). Values are derived with the cross-validation experiment described in the Methods section of the main text. N_{meas} is the number of glaciers for which ice thickness information is reported within GlaThiDa v2. For regions with $N_{\text{meas}} < 5$ (labelled with *), the weights are obtained by pooling all regions. Weights are relative, and are distributed amongst models that actually provide a solution for a given region (i.e. the sum of the weights is 100 % for every region).

RGI region		N_{meas}	M1	M2	M3	M4	M5
01	Alaska	9	45 %	22 %	33 %	-	-
02	Western Canada and US	29	35 %	29 %	35 %	-	-
03	Arctic Canada North	235	35 %	30 %	35 %	-	-
04	Arctic Canada South	24	27 %	32 %	40 %	-	-
05	Greenland Periphery	204	44 %	56 %	-	-	-
06	Iceland	3*	38 %	32 %	30 %	-	-
07	Svalbard ⁽¹⁾	65	-	-	-	(100 %)	-
08	Scandinavia	97	26 %	19 %	25 %	31 %	-
09	Russian Arctic	15	30 %	33 %	37 %	-	-
10	North Asia	20	25 %	39 %	36 %	-	-
11	Central Europe	125	27 %	27 %	12 %	15 %	18 %
12	Caucasus and Middle East	21	31 %	25 %	23 %	-	21 %
13	Central Asia	38	25 %	25 %	20 %	31 %	-
14	South Asia West	0*	31 %	26 %	25 %	-	18 %
15	South Asia East	2*	26 %	22 %	20 %	32 %	-
16	Low Latitudes	4*	38 %	32 %	30 %	-	-
17	Southern Andes	38	41 %	42 %	17 %	-	-
18	New Zealand	2*	26 %	22 %	20 %	32 %	-
19	Antarctic and Subantarctic	69	60 %	40 %	-	-	-
All regions pooled		1000	22 %	19 %	18 %	28 %	13 %

⁽¹⁾ For Svalbard, estimates are taken from Fürst et al. (2018), who used a method similar to M4 (Fürst et al., 2017).

Same weight for every region

Table S 2: Estimated regional glacier ice volumes from this and previous studies. Values are given in mm sea level equivalent (see Methods in the main text). Numbers for this study (a) refer to the composite solution, (b) do not correct for ice portions below present sea level (in line with previous studies but contrary to Table 1 of the main text), and (c) are obtained by assigning the same, pooled weight (see last row of Table S 1) to every RGI region. When previous studies used a different regions nomenclature, correspondence is given in the table's footnotes.

RGI region	This study		Radić and Hock (2010) ⁽¹⁾		Huss and Farinotti (2012)		Marzeion et al. (2012)		Grinsted (2013)		Radić et al. (2014)		Frey et al. (2014) ⁽⁴⁾		Martín-Español et al. (2015)		Average of previous estimates		Difference between this study and average of previous estimates		Difference between this study and Huss and Farinotti (2012)	
01 Alaska	45.8	66.3	49.3	75.1	43.3	67.3	-	-	60.3	(-23.9 %)	[-7.0 %]											
02 Western Canada and US	2.6	4.6	2.5	3.0	2.5	3.1	-	-	3.1	(-18.7 %)	[2.9 %]											
03 Arctic Canada North	68.4	193.6	83.1	100.6	59.9	134.1	-	-	114.3	(-40.1 %)	[-17.6 %]											
04 Arctic Canada South	20.8	- ⁽²⁾	23.7	20.2	14.8	22.6	-	-	20.3	(2.4 %)	[-12.3 %]											
05 Greenland Periphery	37.9	43.1	46.0	26.8	45.7	41.4	-	-	40.6	(-6.6 %)	[-17.6 %]											
06 Iceland	9.1	11.8	10.7	12.4	8.5	6.4	-	-	10.0	(-8.7 %)	[-15.1 %]											
07 Svalbard	18.0	24.8	23.4	21.5	12.9	22.0	-	16.2	20.1	(-10.3 %)	[-22.9 %]											
08 Scandinavia	0.7	0.5	0.6	0.6	0.8	0.5	-	-	0.6	(20.2 %)	[16.4 %]											
09 Russian Arctic	35.4	42.8	40.7	57.1	32.8	42.9	-	-	43.3	(-18.3 %)	[-13.1 %]											
10 North Asia	0.3	0.4	0.3	0.6	0.5	0.7	-	-	0.5	(-34.1 %)	[-3.6 %]											
11 Central Europe	0.3	0.5	0.3	0.3	0.3	0.3	-	-	0.3	(-8.0 %)	[8.5 %]											
12 Caucasus and Middle East	0.2	0.2	0.1	0.2	0.2	0.2	-	-	0.2	(-16.0 %)	[3.3 %]											
13 Central Asia	7.9	30.1	12.1	15.2	23.0	15.7	-	-	19.2	(-58.9 %)	[-34.9 %]											
14 South Asia West	6.9	- ⁽³⁾	7.8	9.2	9.2	10.8	6.8	-	8.8	(-21.2 %)	[-11.6 %]											
15 South Asia East	2.1	- ⁽³⁾	3.2	3.7	4.0	4.5	2.2	-	3.5	(-39.4 %)	[-33.2 %]											
16 Low Latitudes	0.2	0.8	0.3	0.6	0.3	0.6	-	-	0.5	(-54.6 %)	[-31.9 %]											
17 Southern Andes	12.9	19.6	16.1	12.4	11.4	16.5	-	-	15.2	(-15.2 %)	[-20.0 %]											
18 New Zealand	0.2	0.2	0.2	0.2	0.3	0.2	-	-	0.2	(-15.1 %)	[4.3 %]											
19 Antarctic and Subantarctic	112.2	143.8	90.6	-	73.0	117.5	-	-	106.2	(5.7 %)	[23.9 %]											
TOTAL	381.9	583.1	411.0	359.7	343.4	507.3	-	-	467.2	(-18.2 %)	[-7.1 %]											
Arctic (03+04+05+07+09)	180.5	304.3	216.9	226.2	166.1	263.0	-	-	238.6	(-24.4 %)	[-16.8 %]											
Antarctic (19)	112.2	143.8	90.6	-	73.0	117.5	-	-	106.2	(5.6 %)	[23.8 %]											
Alaska (01)	45.8	66.3	49.3	75.1	43.3	67.3	-	-	60.3	(-24.0 %)	[-7.1 %]											
High Mountain Asia (13+14+15)	16.9	30.1	23.1	28.1	36.2	31.0	-	-	31.5	(-46.3 %)	[-26.8 %]											
Other (9 regions)	26.5	38.6	31.1	30.3	24.8	28.5	-	-	30.6	(-13.4 %)	[-14.8 %]											

⁽¹⁾ Regions nomenclature: RGI region (Reg.) 10 = Franz Josef Land + Novaya Zemlya + Severnaya Zemlya; Reg. 16 = South America I; Reg. 17 = South America II; Reg. 19 = Sub-Antarctic islands + Antarctica

⁽²⁾ Volume accounted for within Reg. 04.

⁽³⁾ Volume accounted for within Reg. 13.

⁽⁴⁾ Regions nomenclature: Reg. 14 = Karakoram + West Himalayas; Reg. 15 = Central Himalayas + East Himalayas

Regionally differentiated weights

Table S 3: Same as Table S 2, but for the case in which regionally differentiated weights (see Table S 1) are assigned to individual models.

RGI region	This study	Radić and Hock (2010) ⁽¹⁾		Huss and Farinotti (2012)		Marzeion et al. (2012)		Grinsted (2013)		Radić et al. (2014)		Frey et al. (2014) ⁽⁴⁾		Martín-Español et al. (2015)	Average of previous estimates	Difference between this study and average of previous estimates	Difference between this study and Huss and Farinotti (2012)
01 Alaska	45.5	66.3	49.3	75.1	43.3	67.3	-	-	-	60.3	(-24.4 %)	[-7.6 %]	-	-	-	-	
02 Western Canada and US	2.6	4.6	2.5	3.0	2.5	3.1	-	-	-	3.1	(-18.2 %)	[3.5 %]	-	-	-	-	
03 Arctic Canada North	68.0	193.6	83.1	100.6	59.9	134.1	-	-	-	114.3	(-40.5 %)	[-18.1 %]	-	-	-	-	
04 Arctic Canada South	20.4	- ⁽²⁾	23.7	20.2	14.8	22.6	-	-	-	20.3	(0.6 %)	[-13.8 %]	-	-	-	-	
05 Greenland Periphery	37.8	43.1	46.0	26.8	45.7	41.4	-	-	-	40.6	(-6.8 %)	[-17.7 %]	-	-	-	-	
06 Iceland	9.1	11.8	10.7	12.4	8.5	6.4	-	-	-	10.0	(-8.6 %)	[-15.1 %]	-	-	-	-	
07 Svalbard	18.0	24.8	23.4	21.5	12.9	22.0	-	-	16.2	20.1	(-10.3 %)	[-22.9 %]	-	-	-	-	
08 Scandinavia	0.7	0.5	0.6	0.6	0.8	0.5	-	-	-	0.6	(21.4 %)	[17.6 %]	-	-	-	-	
09 Russian Arctic	35.0	42.8	40.7	57.1	32.8	42.9	-	-	-	43.3	(-19.1 %)	[-14.0 %]	-	-	-	-	
10 North Asia	0.3	0.4	0.3	0.6	0.5	0.7	-	-	-	0.5	(-34.6 %)	[-4.3 %]	-	-	-	-	
11 Central Europe	0.3	0.5	0.3	0.3	0.3	0.3	-	-	-	0.3	(-10.1 %)	[6.0 %]	-	-	-	-	
12 Caucasus and Middle East	0.2	0.2	0.1	0.2	0.2	0.2	-	-	-	0.2	(-17.3 %)	[1.6 %]	-	-	-	-	
13 Central Asia	7.8	30.1	12.1	15.2	23.0	15.7	-	-	-	19.2	(-59.2 %)	[35.4 %]	-	-	-	-	
14 South Asia West	6.9	- ⁽³⁾	7.8	9.2	9.2	10.8	6.8	-	-	8.8	(-21.3 %)	[-11.8 %]	-	-	-	-	
15 South Asia East	2.1	- ⁽³⁾	3.2	3.7	4.0	4.5	2.2	-	-	3.5	(-39.8 %)	[-33.6 %]	-	-	-	-	
16 Low Latitudes	0.2	0.8	0.3	0.6	0.3	0.6	-	-	-	0.5	(-54.6 %)	[-31.9 %]	-	-	-	-	
17 Southern Andes	12.9	19.6	16.1	12.4	11.4	16.5	-	-	-	15.2	(-15.0 %)	[-19.8 %]	-	-	-	-	
18 New Zealand	0.2	0.2	0.2	0.2	0.3	0.2	-	-	-	0.2	(-12.8 %)	[7.1 %]	-	-	-	-	
19 Antarctic and Subantarctic	112.3	143.8	90.6	-	73.0	117.5	-	-	-	106.2	(5.8 %)	[24.0 %]	-	-	-	-	
TOTAL	380.3	583.1	411.0	359.7	343.4	507.3	-	-	-	467.2	(-18.5 %)	[-7.4 %]	-	-	-	-	
Arctic (03+04+05+07+09)	179.2	304.3	216.9	226.2	166.1	263.0	-	-	-	238.6	(-24.9 %)	[-17.4 %]	-	-	-	-	
Antarctic (19)	112.3	143.8	90.6	-	73.0	117.5	-	-	-	106.2	(5.7 %)	[24.0 %]	-	-	-	-	
Alaska (01)	45.5	66.3	49.3	75.1	43.3	67.3	-	-	-	60.3	(-24.5 %)	[-7.7 %]	-	-	-	-	
High Mountain Asia (13+14+15)	16.8	30.1	23.1	28.1	36.2	31.0	-	-	-	31.5	(-46.7 %)	[-27.3 %]	-	-	-	-	
Other (9 regions)	26.5	38.6	31.1	30.3	24.8	28.5	-	-	-	30.6	(-13.4 %)	[-14.8 %]	-	-	-	-	

⁽¹⁾ Regions nomenclature: RGI region (Reg.) 10 = Franz Josef Land + Novaya Zemlya + Severnaya Zemlya;

Reg. 16 = South America I; Reg. 17 = South America II; Reg. 19 = Sub-Antarctic islands + Antarctica

⁽²⁾ Volume accounted for within Reg. 04.

⁽³⁾ Volume accounted for within Reg. 13.

⁽⁴⁾ Regions nomenclature: Reg. 14 = Karakoram + West Himalayas; Reg. 15 = Central Himalayas + East Himalayas

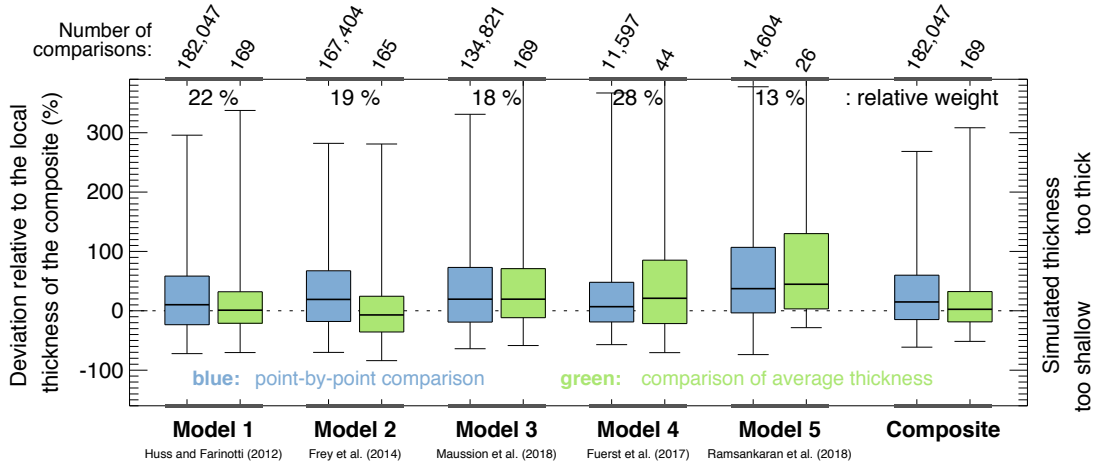


Figure S1: Assessment of model performance. The distribution of the relative deviations between modelled and measured ice thickness is shown for every model and for the composite solution. Deviations are given relative to the ice thickness of the composite and refer to point-by-point comparisons (blue) or comparisons of the average thickness (green). The number of points composing each box plot is given above the plot. Box plots show the 95% confidence interval (whiskers), the interquartile range (box), and the median (lines within box). "Relative weight" refers to the weight assigned to individual models when producing the composite solution (cf. Methods in the main text and Table S1).

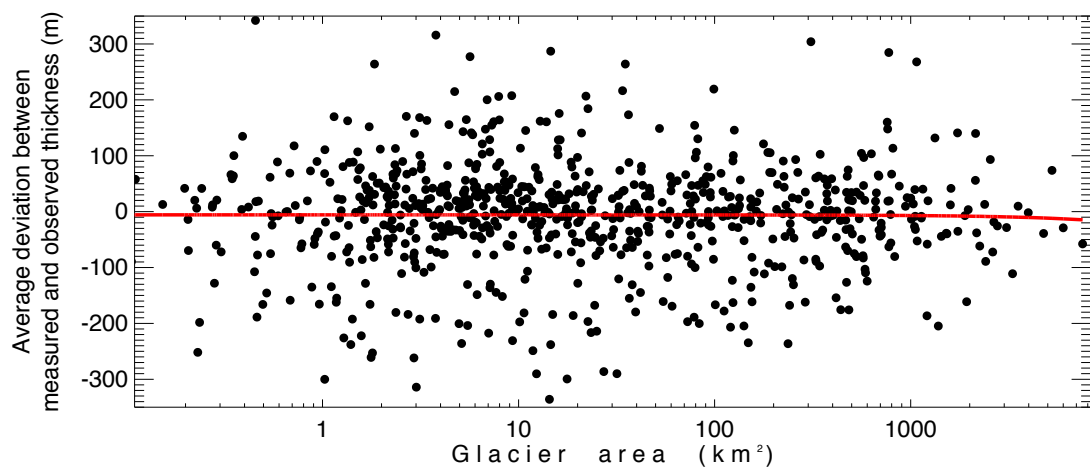


Figure S 2: Assessment of possible bias in the results. The mean deviation between measured and observed ice thickness is shown as a function of glacier size. The red line is a linear fit through all points, and shows no discernible trend. Note the logarithmic scale for glacier area.

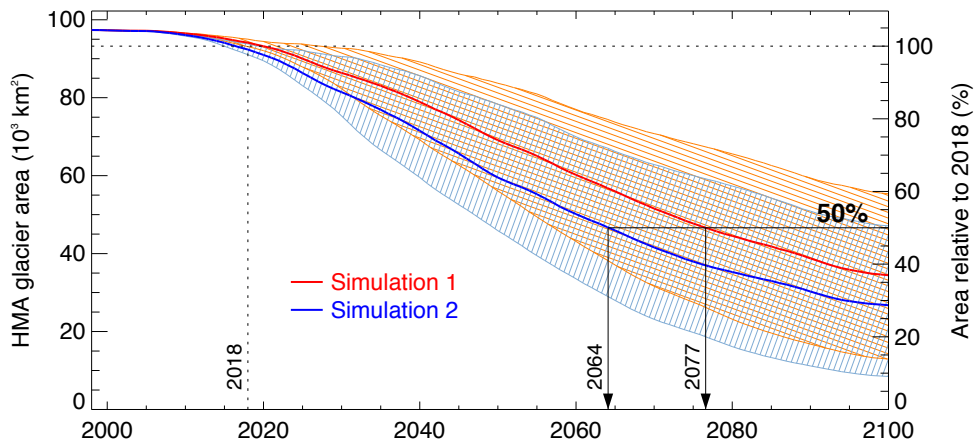


Figure S 3: Implication of the estimated present-day ice thickness on the projected glacier area evolution for High Mountain Asia (RGI regions 13+14+15). Projections are based on the Global Glacier Evolution Model (GloGEM; see Huss and Hock, 2015, and "Methods" section of the main text), which was forced with the output of 14 different climate models under Representative Concentration Pathway 4.5 (Meinshausen et al., 2011). Simulation 1 and 2 are based on the ice thickness distribution presented by Huss and Farinotti (2012) and this study, respectively. Thick lines represent the ensemble median, whilst the bands are 95 % confidence intervals. The time by which 50 % of the present-day (year 2018) glacier area has shrunk by 50 % is marked.

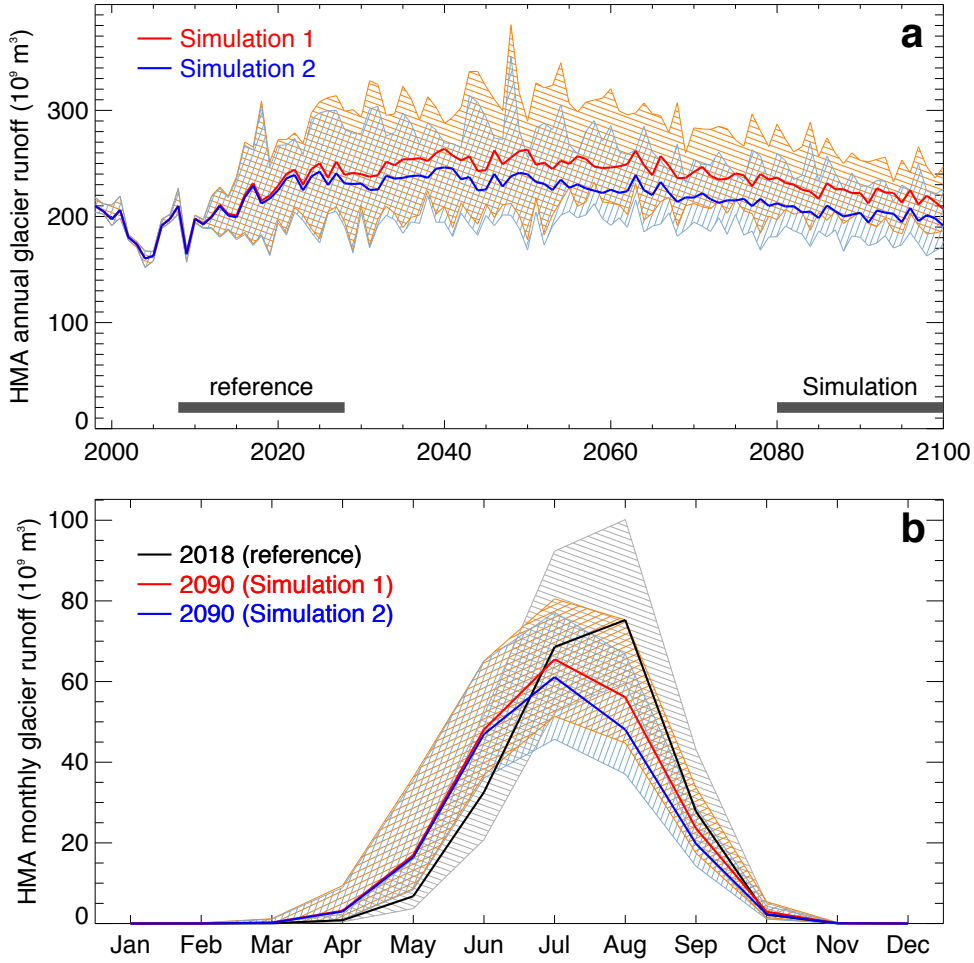


Figure S4: Implication of the estimated present-day ice thickness on the projected glacier runoff evolution for High Mountain Asia (RGI regions 13+14+15). (a) Total annual glacier runoff. (b) Monthly glacier runoff averaged over a 20-year period around the indicated year (see also horizontal bars in panel a). Projections are based on the Global Glacier Evolution Model (GloGEM; see Huss and Hock, 2015, and "Methods" section of the main text), which was forced with the output of 14 different climate models under Representative Concentration Pathway 4.5 (Meinshausen et al., 2011). Simulation 1 and 2 are based on the ice thickness distribution presented by Huss and Farinotti (2012) and this study, respectively. Thick lines represent the ensemble median, whilst the bands are 95 % confidence intervals.

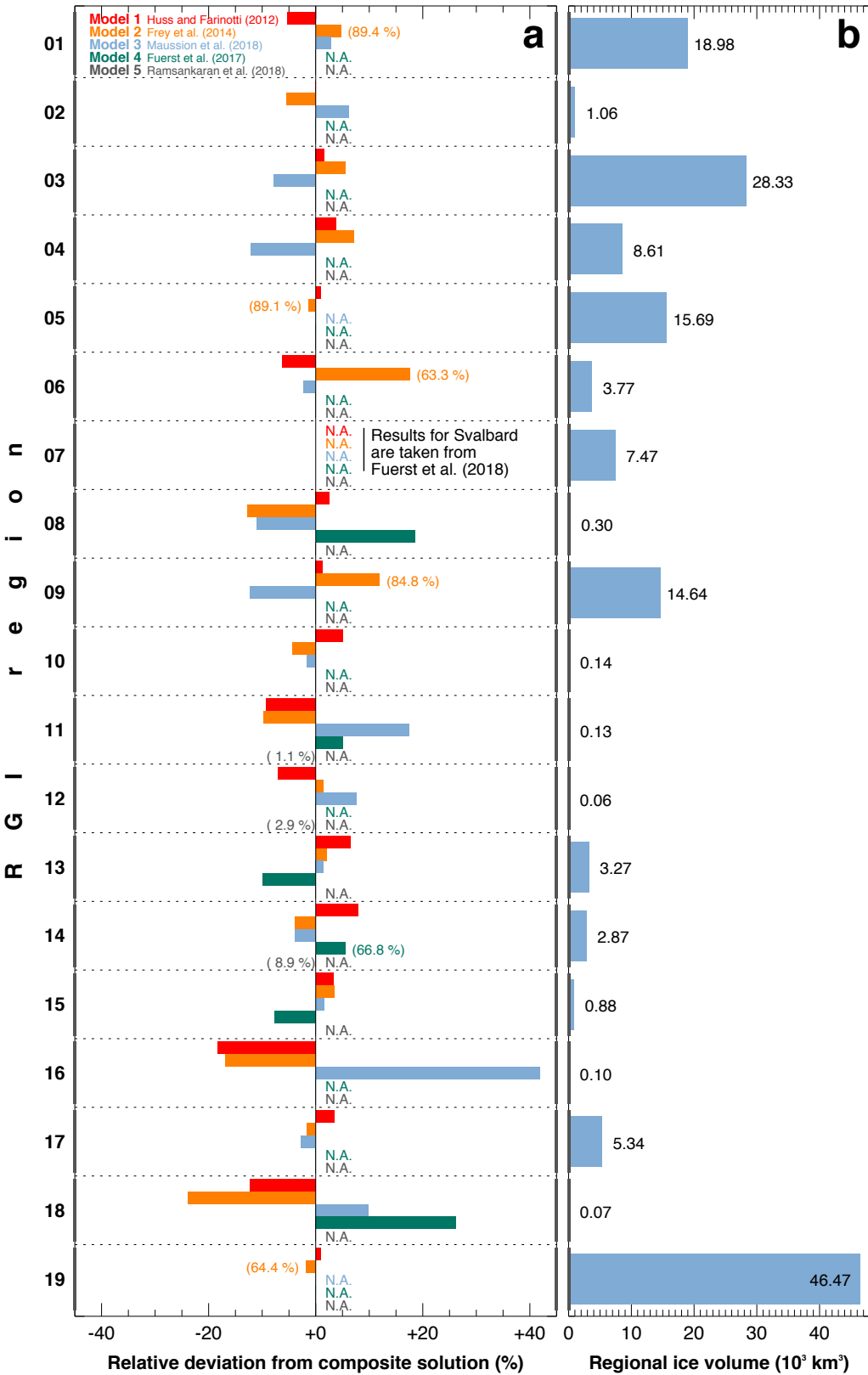


Figure S5: (a) Difference with respect to the composite solution of the ice volume estimated by individual models for the 19 regions of the Randolph Glacier Inventory (RGI). The difference is only shown if the corresponding model considered at least 50 % of the regional glacier area (cf. Fig. 1a in the main text), and only refers to the portion of area actually considered (given within parenthesis if <95 %). (b) Total ice volume as estimated by the composite solution.

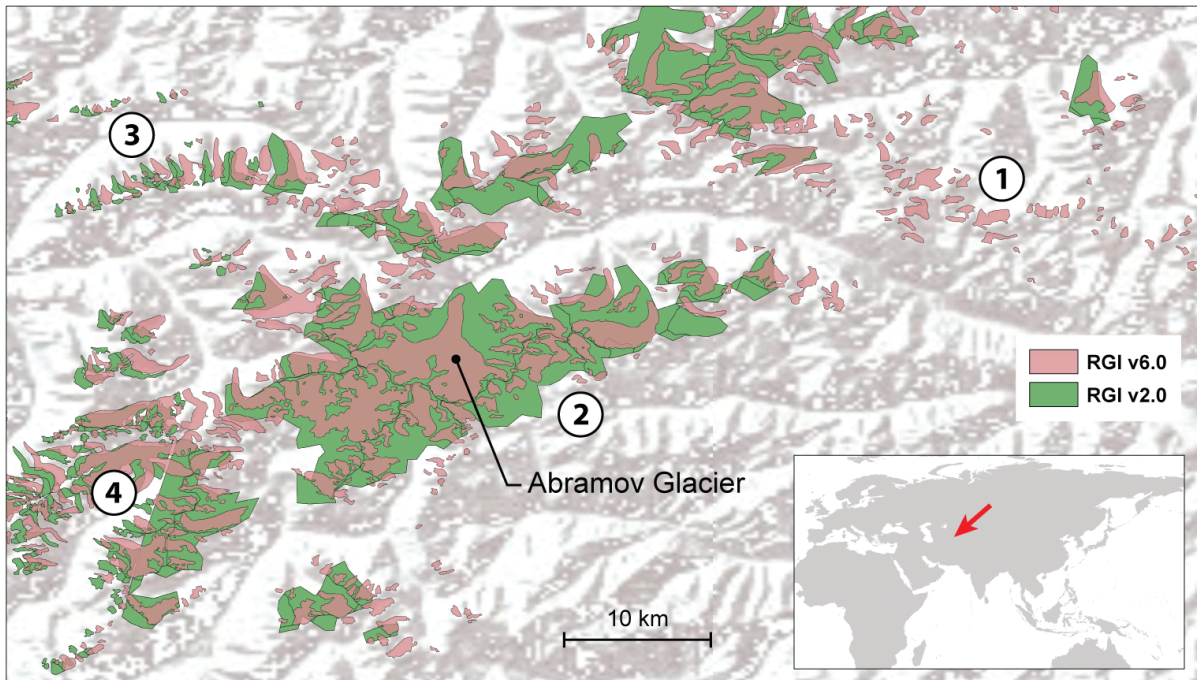


Figure S 6: Example for glacier outline changes between RGI version 2.0 (used by Huss and Farinotti, 2012) and RGI version 6.0 (used in this study). The example refers to the region of Abramov Glacier (labeled), Central Asia. The circled numbers highlight regions for which (1) previously missing glaciers are now inventoried, (2) glacier complexes have been subdivided, (3) geolocation was improved, and (4) artifacts were corrected.

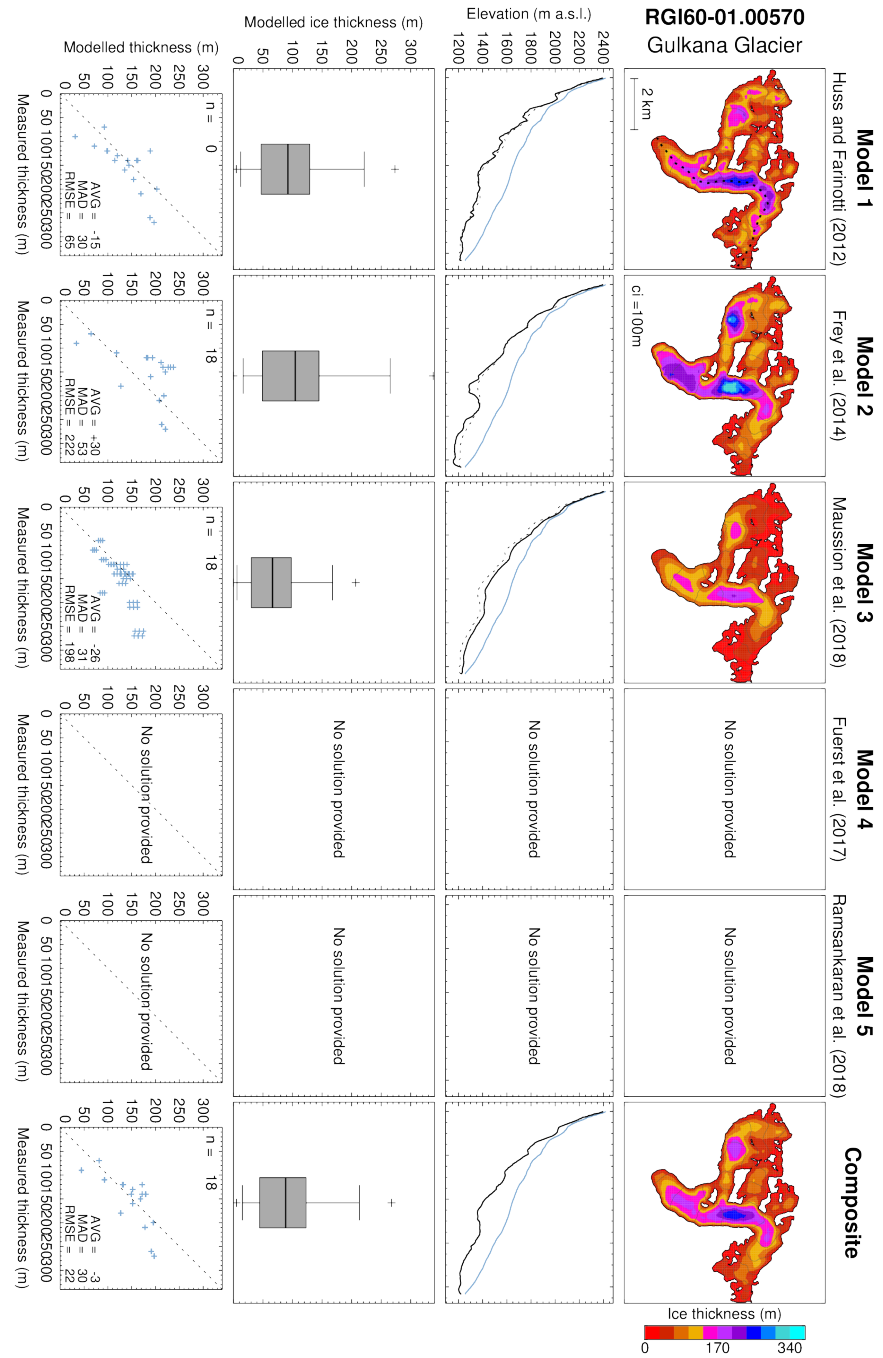


Figure S 7: Example for the estimated ice thickness distribution. The example is arbitrary, and refers to glacier RGI60-01.00570 (RGI region "Alaska"). Rows show the following: (1) Ice thickness distribution as estimated by the various models (Model1 to 5), and the composite. Contour lines refer to surface topography (the contour interval ci is given in the second panel). (2) Longitudinal profile of the glacier surface (blue) and the estimated bedrock topography (solid black). The composite solution (dashed black) is given as a reference. The profile's location is shown in the first panel of the first row (dashed line). (3) Distribution of the estimated ice thickness. Boxplots show minimum and maximum values (crosses), 95% confidence intervals (whiskers), interquartile ranges (box), and medians (line within box). The mean ice thickness reported in GlaThiDa v2.0 (WGMS, 2016) is given when available (asterisk). (4) Scatter-plot between measured and modelled point (blue markers) and mean (asterisk) ice thickness. The following information is given: number of point measurements (n), average deviation (AVG), mean absolute deviation (MAD), root mean square error ($RMSE$). The scatter-plots show pooled data from the cross-validation experiment (see Methods in the main text). All other panels show the final solution.

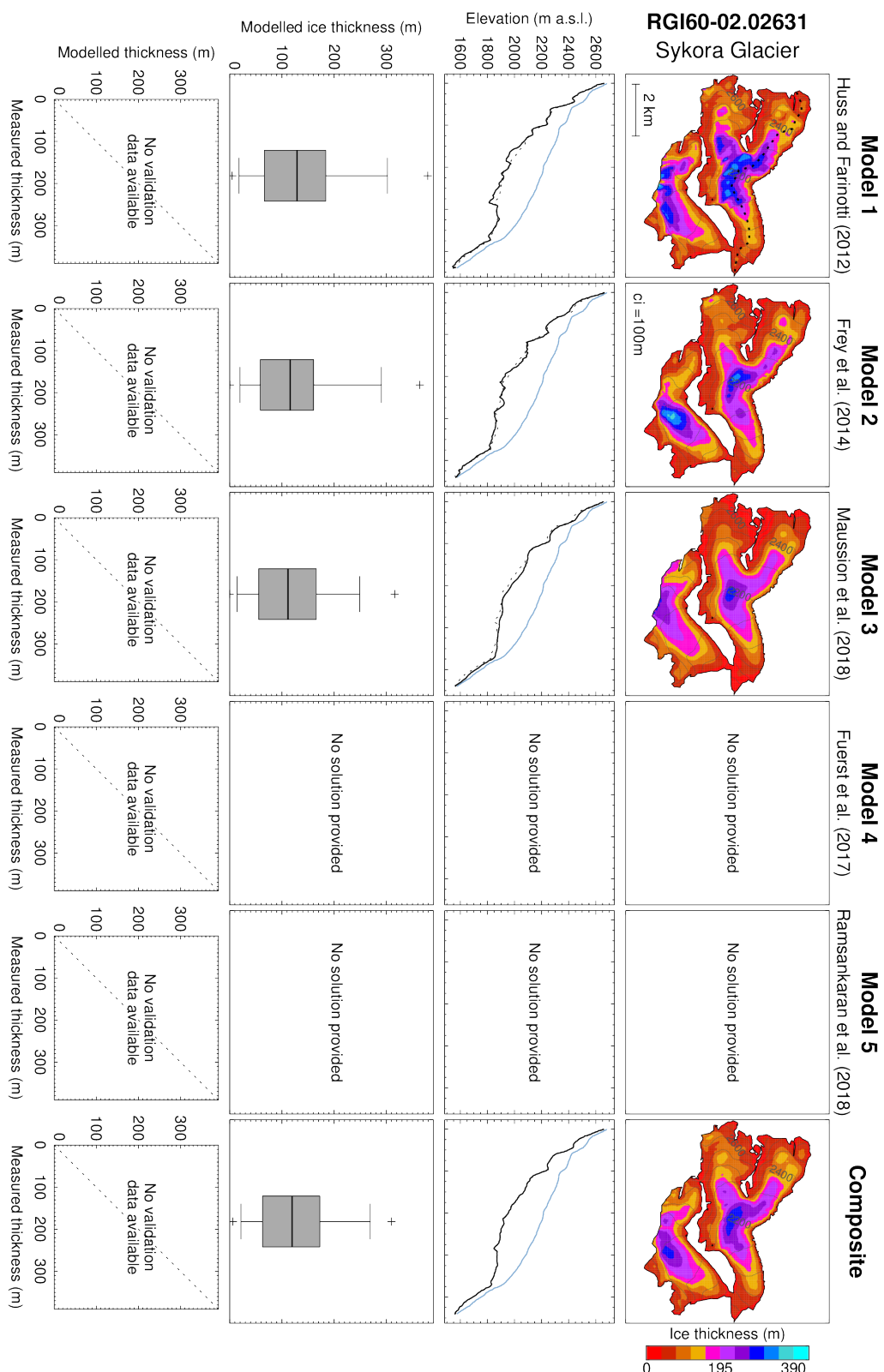


Figure S 8: Same as Figure S 7 but for glacier RGI60-02.02631 (RGI region "Western Canada and US").

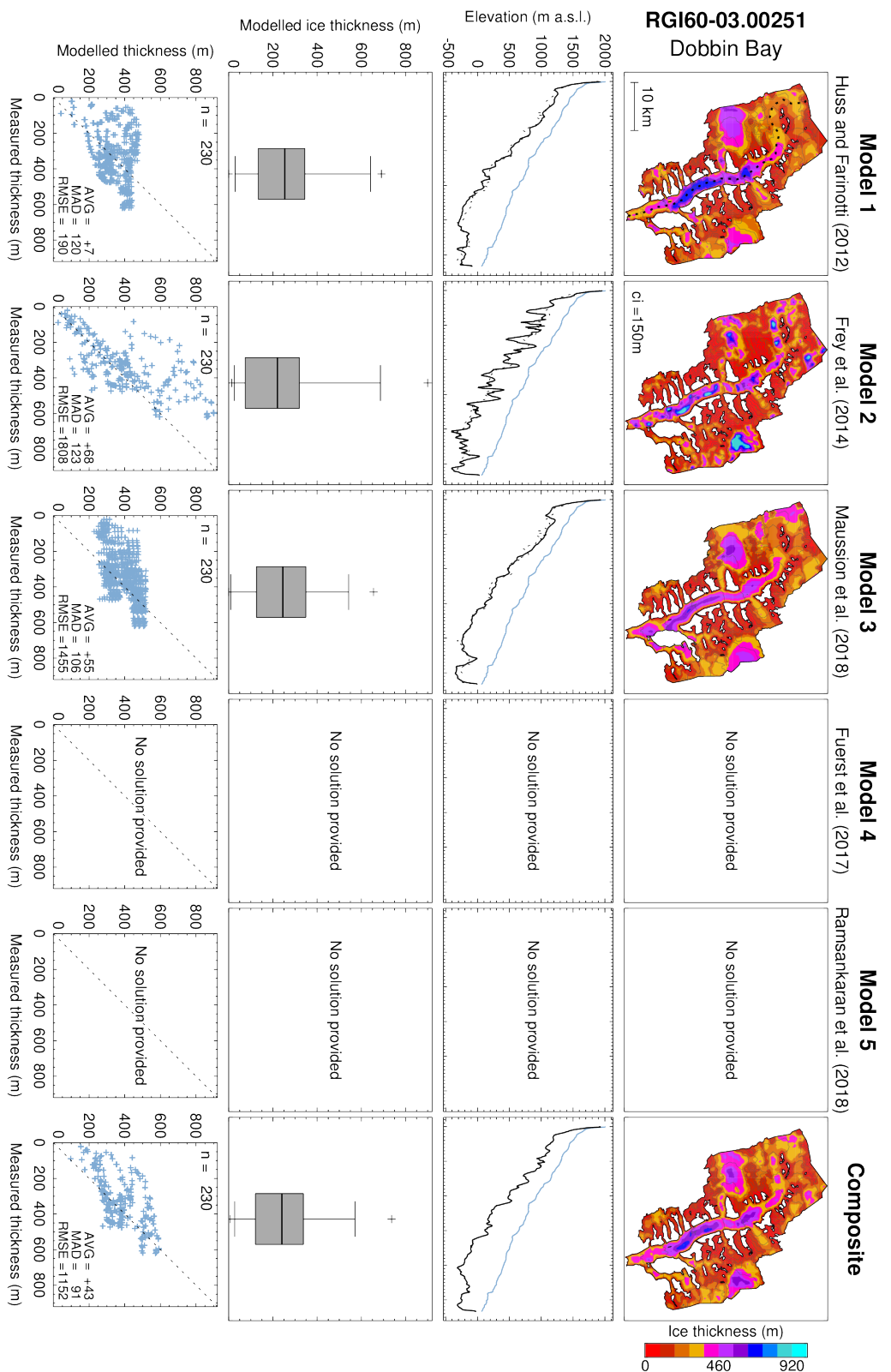


Figure S 9: Same as Figure S 7 but for glacier RGI60-03.00251 (RGI region "Arctic Canada North").

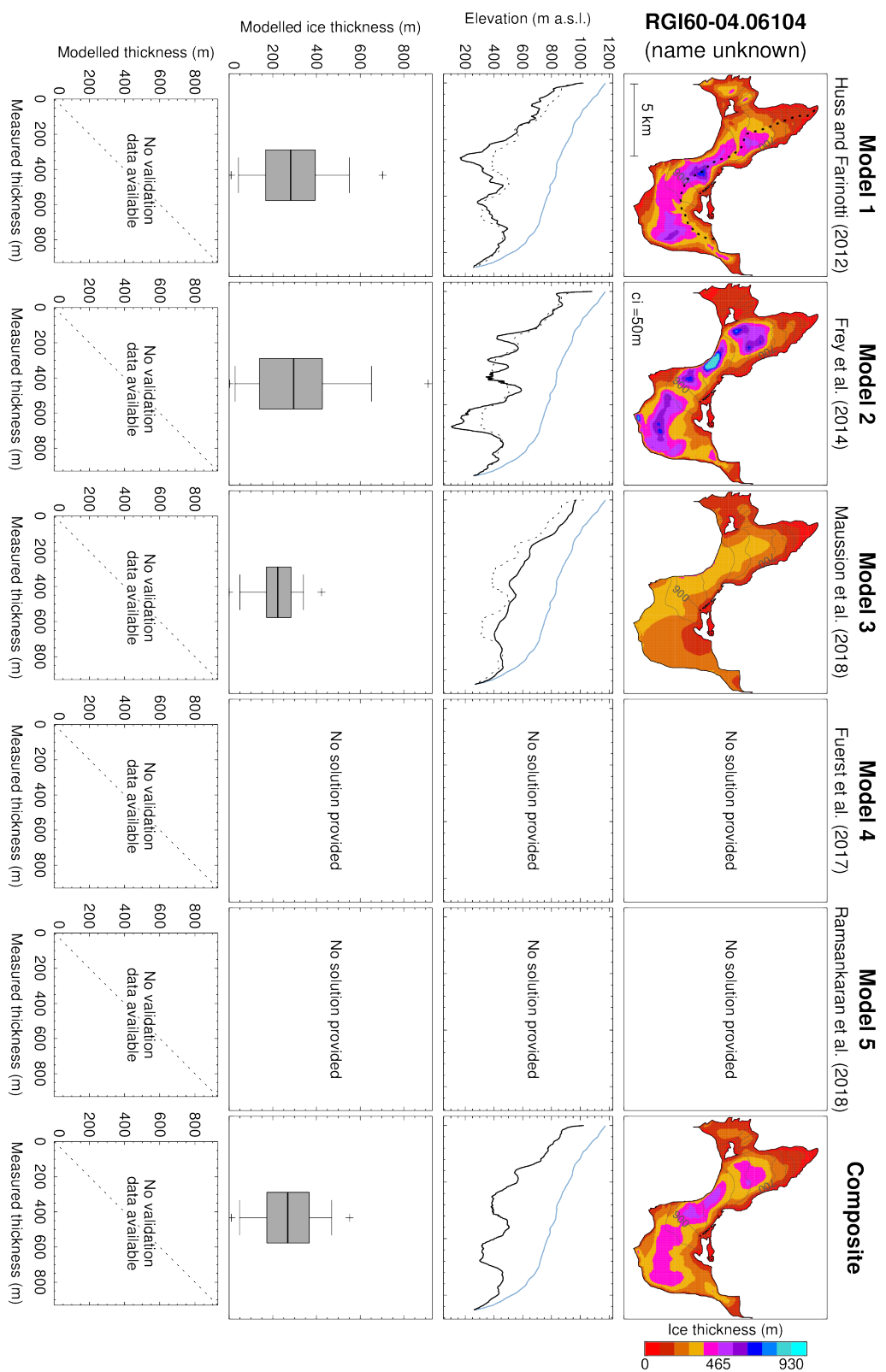


Figure S 10: Same as Figure S 7 but for glacier RGI60-04.06104 (RGI region "Arctic Canada South").

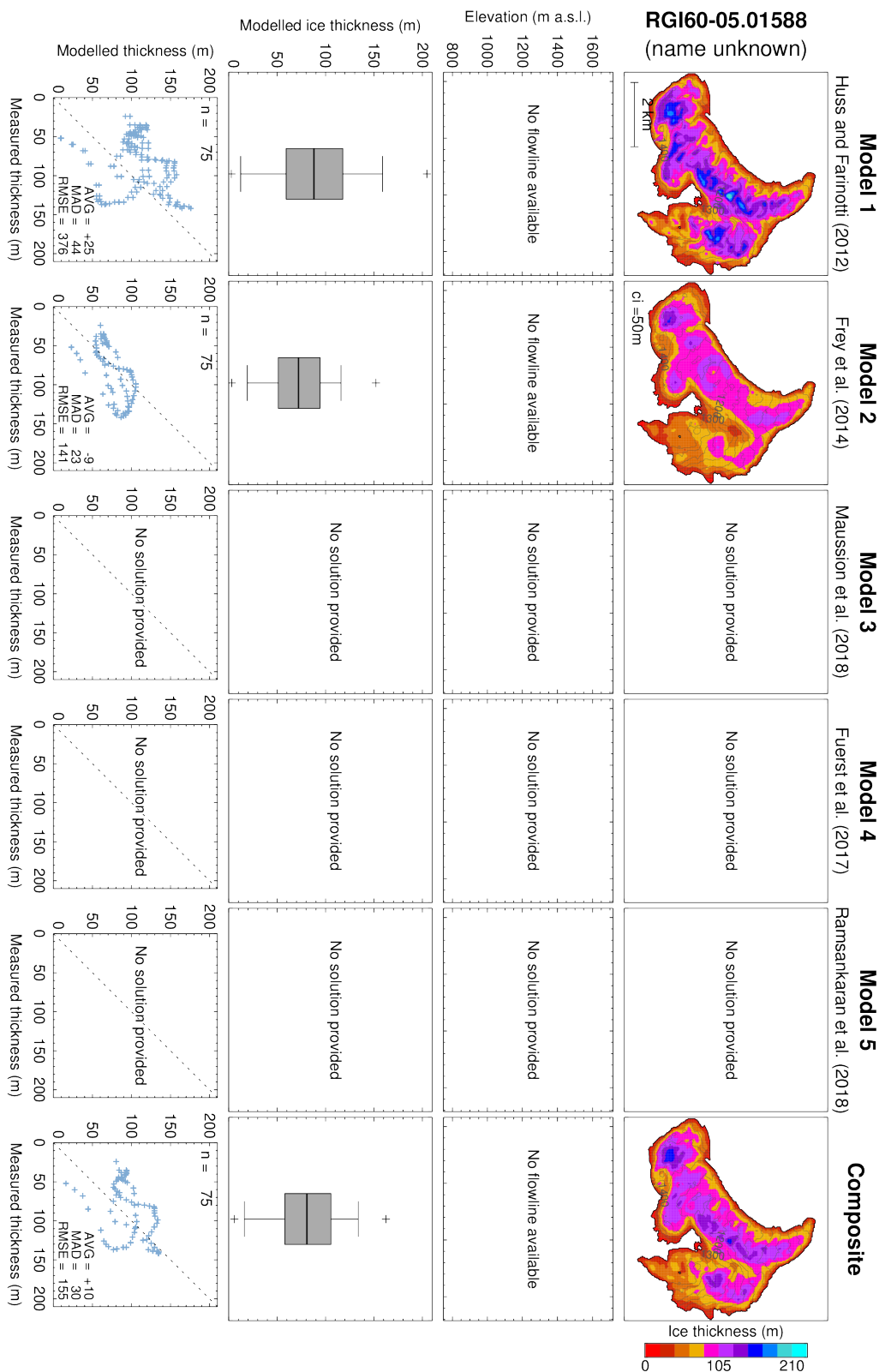
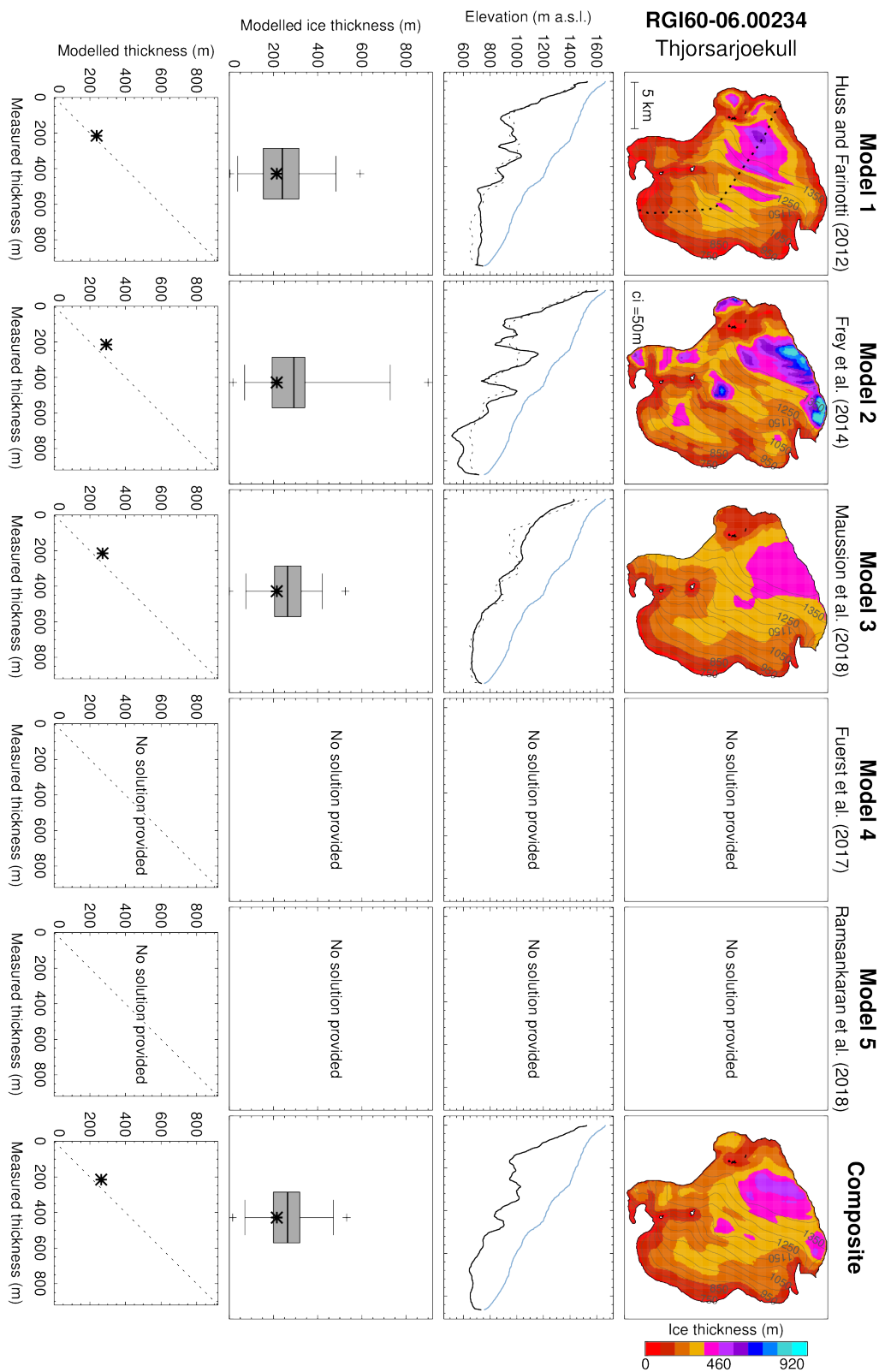


Figure S 11: Same as Figure S 7 but for glacier RGI60-05.01588 (RGI region "Greenland Periphery").



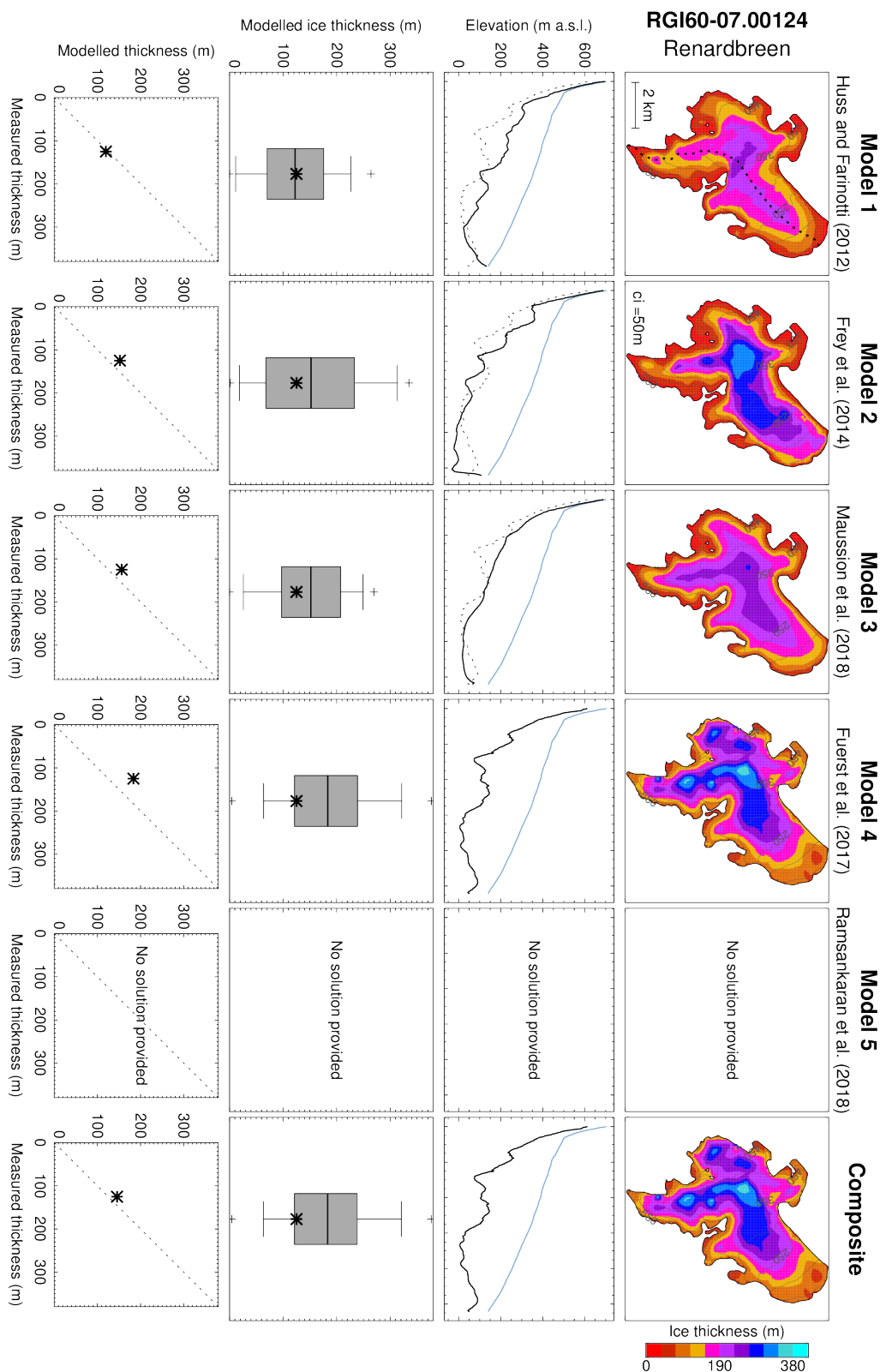


Figure S 13: Same as Figure S 7 but for glacier RGI60-07.00124 (RGI region "Svalbard").

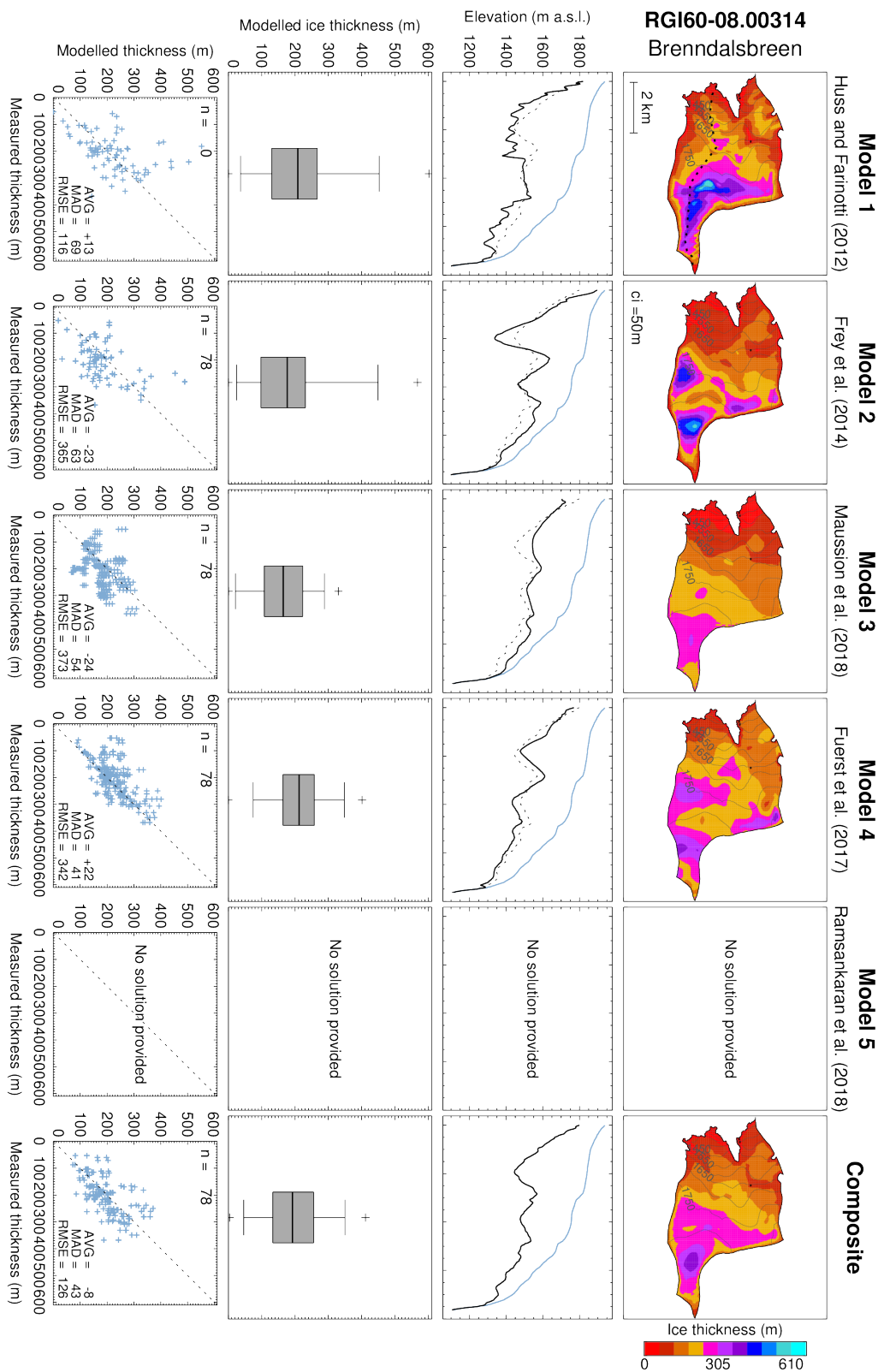
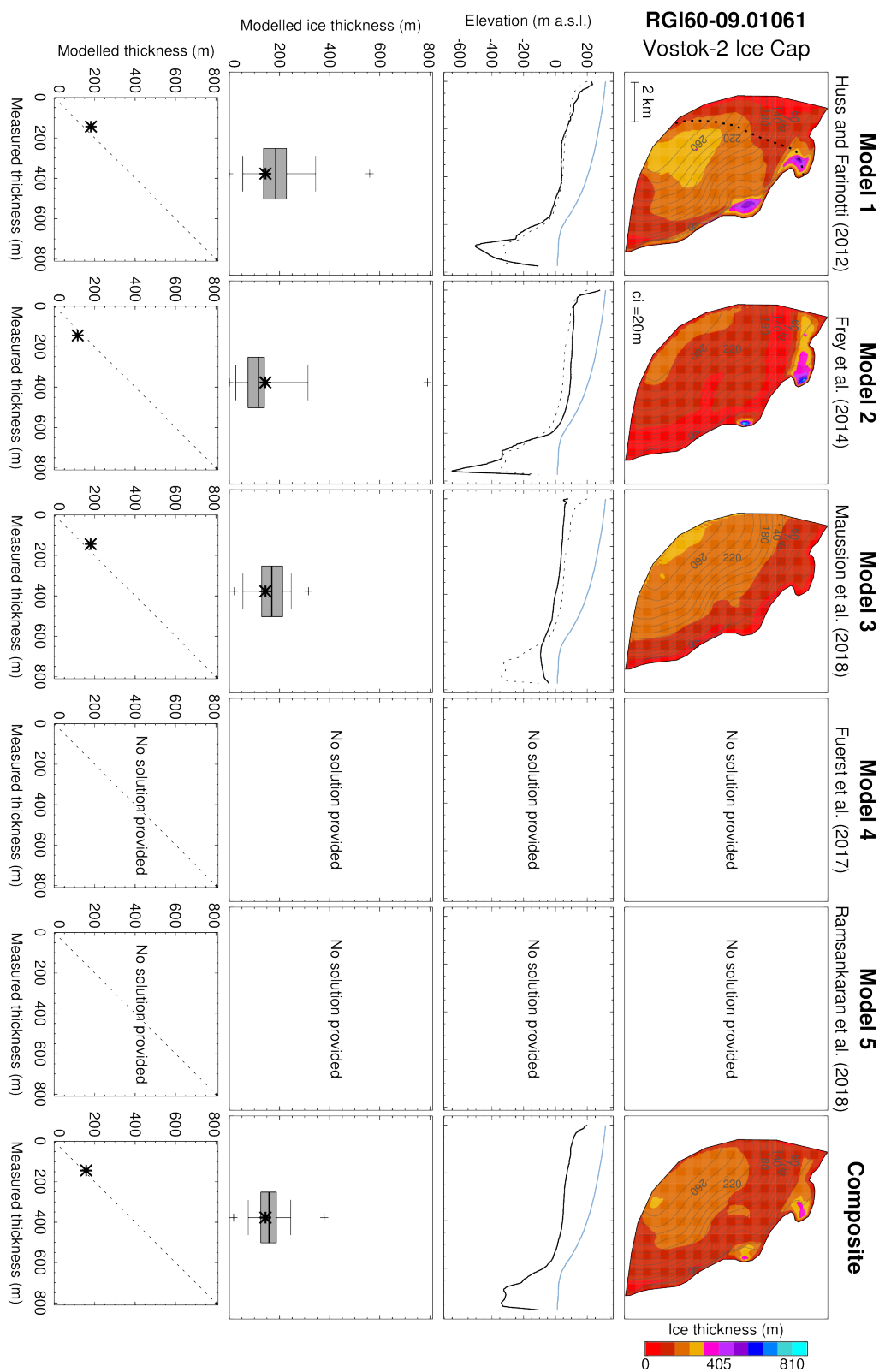


Figure S 14: Same as Figure S 7 but for glacier RGI60-08.00314 (RGI region "Scandinavia").



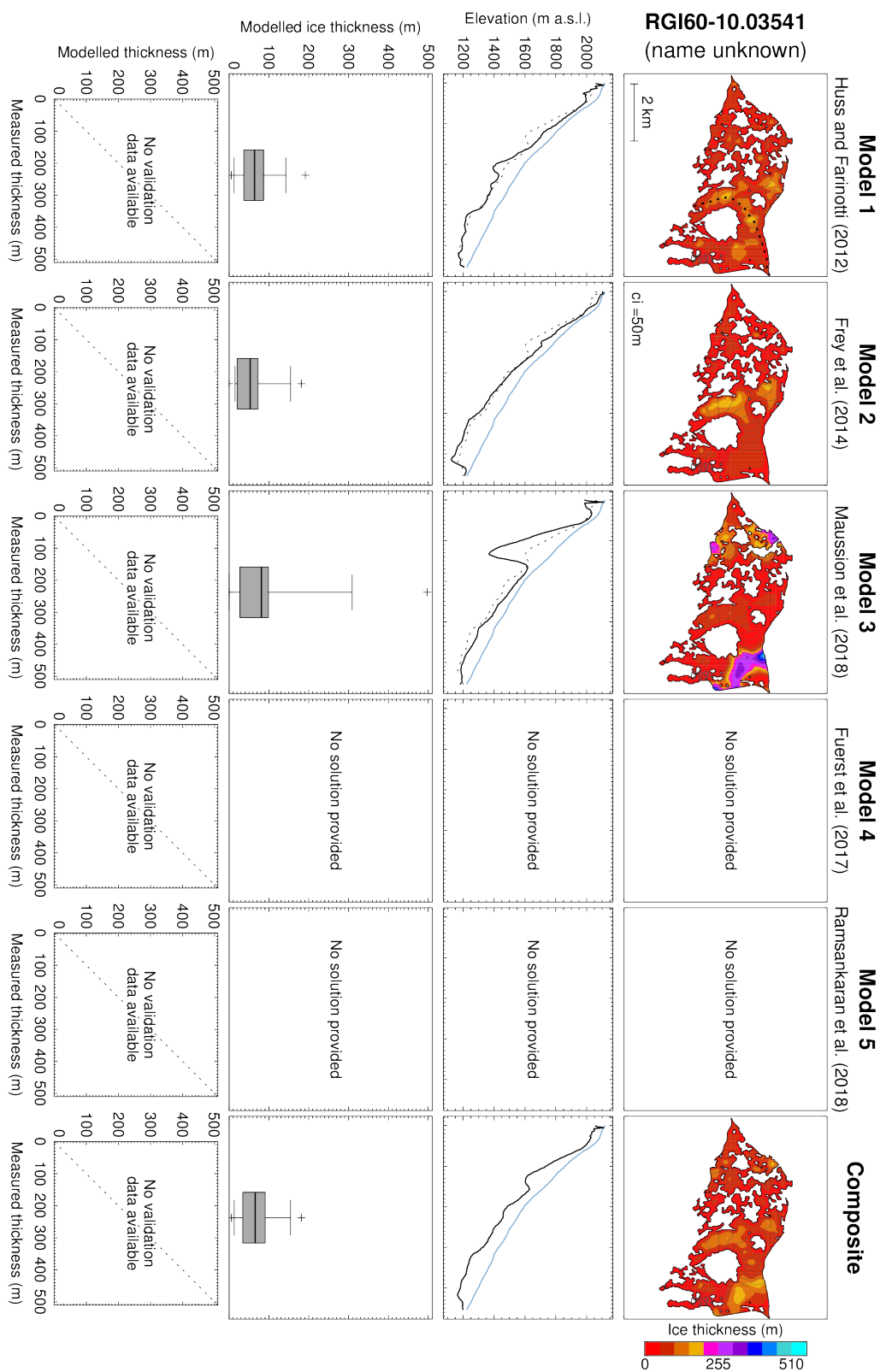


Figure S 16: Same as Figure S 7 but for glacier RGI60-10.03541 (RGI region "North Asia").

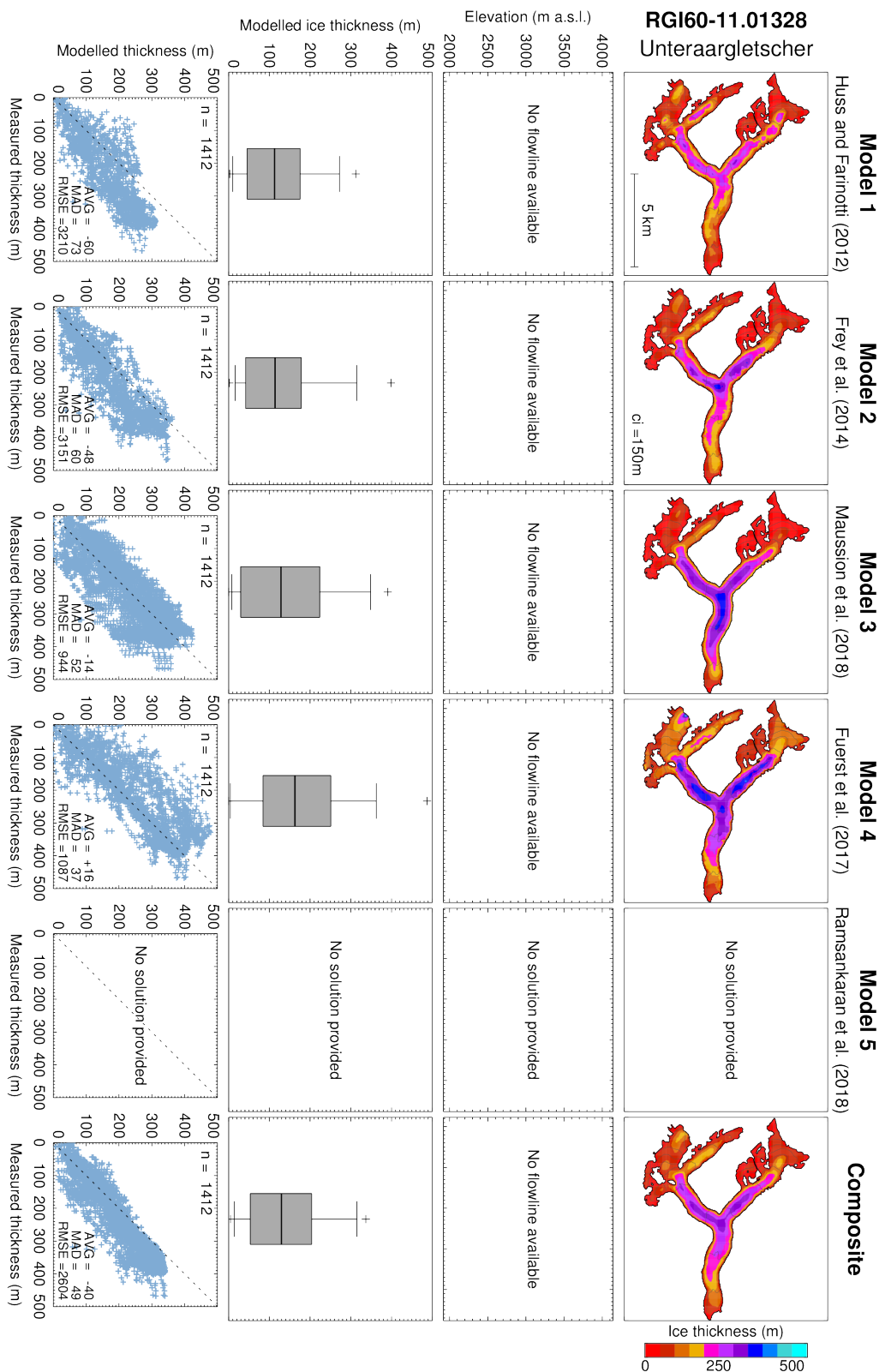


Figure S 17: Same as Figure S 7 but for glacier RGI60-11.01328 (RGI region "Central Europe").

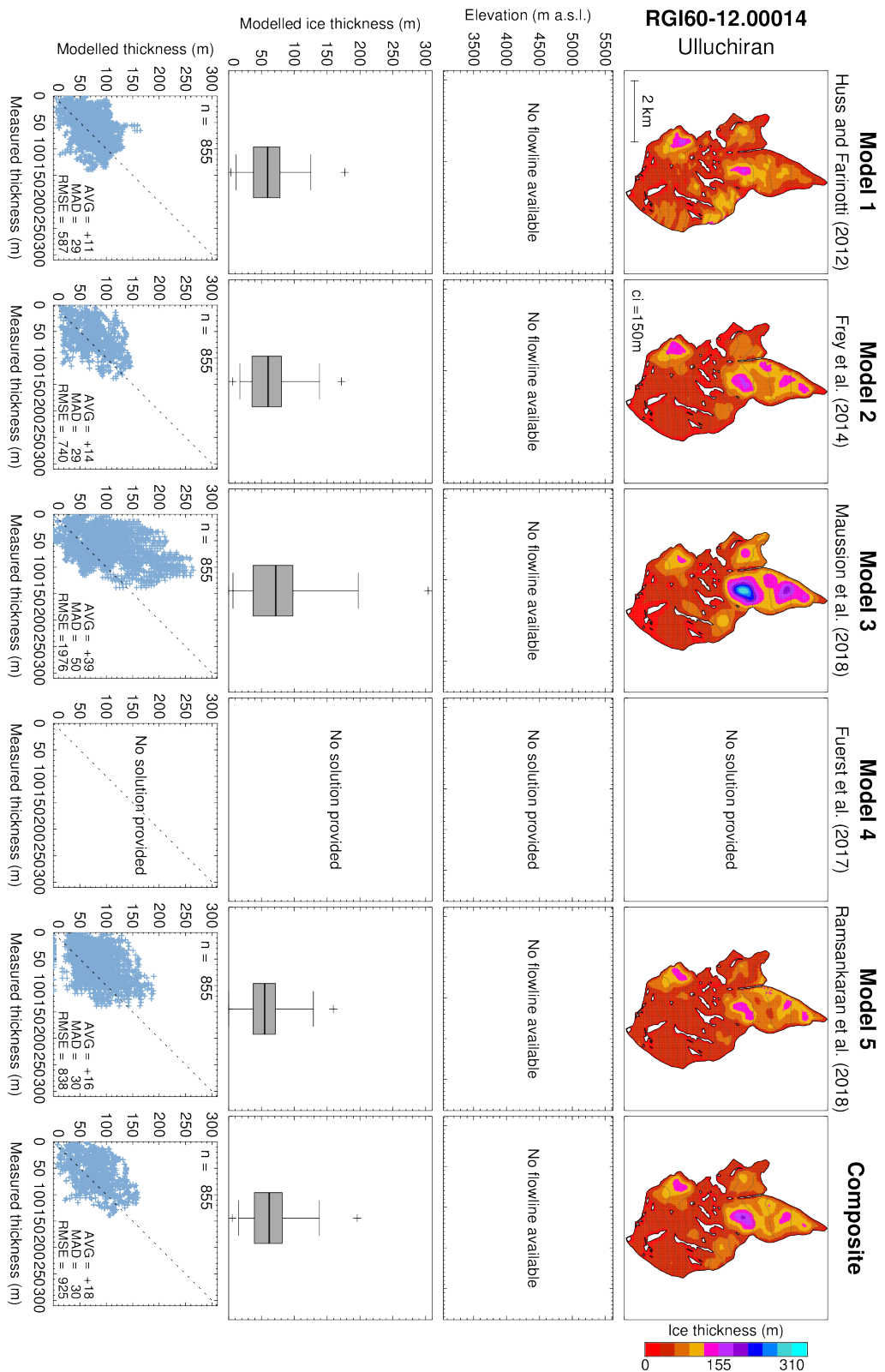
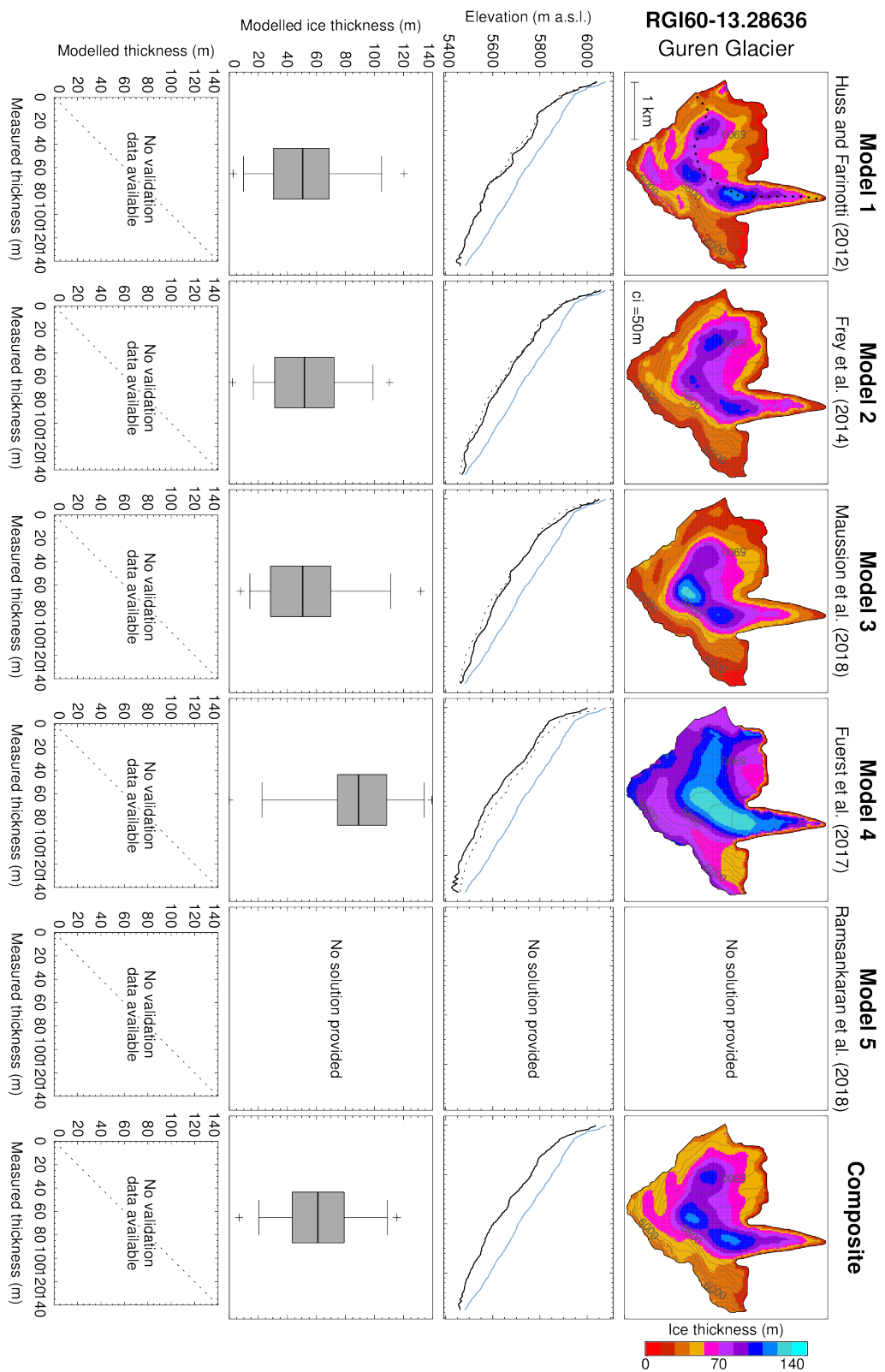


Figure S 18: Same as Figure S 7 but for glacier RGI60-12.00014 (RGI region "Caucasus and Middle East").



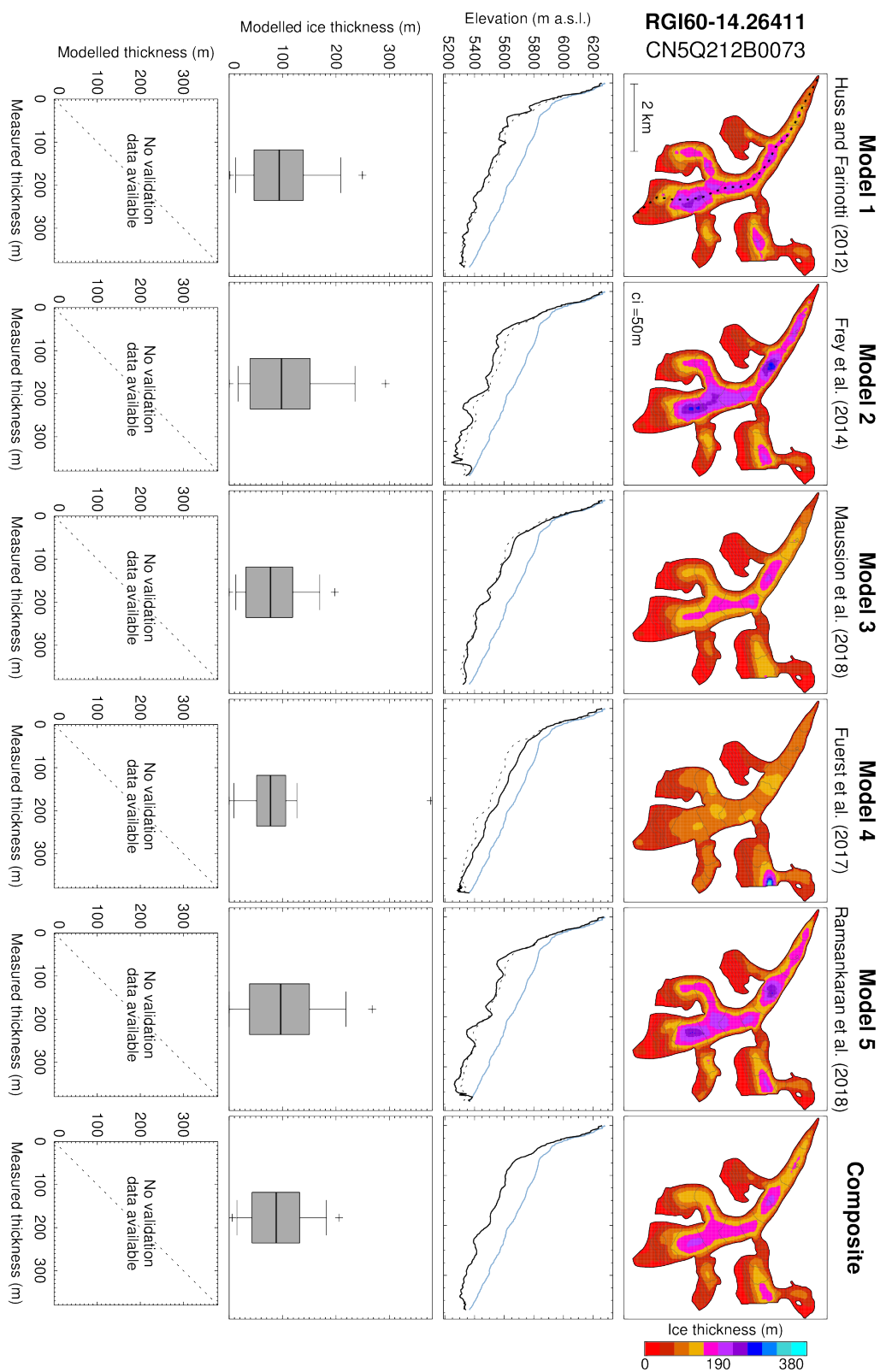


Figure S 20: Same as Figure S 7 but for glacier RGI60-14.26411 (RGI region "South Asia West").

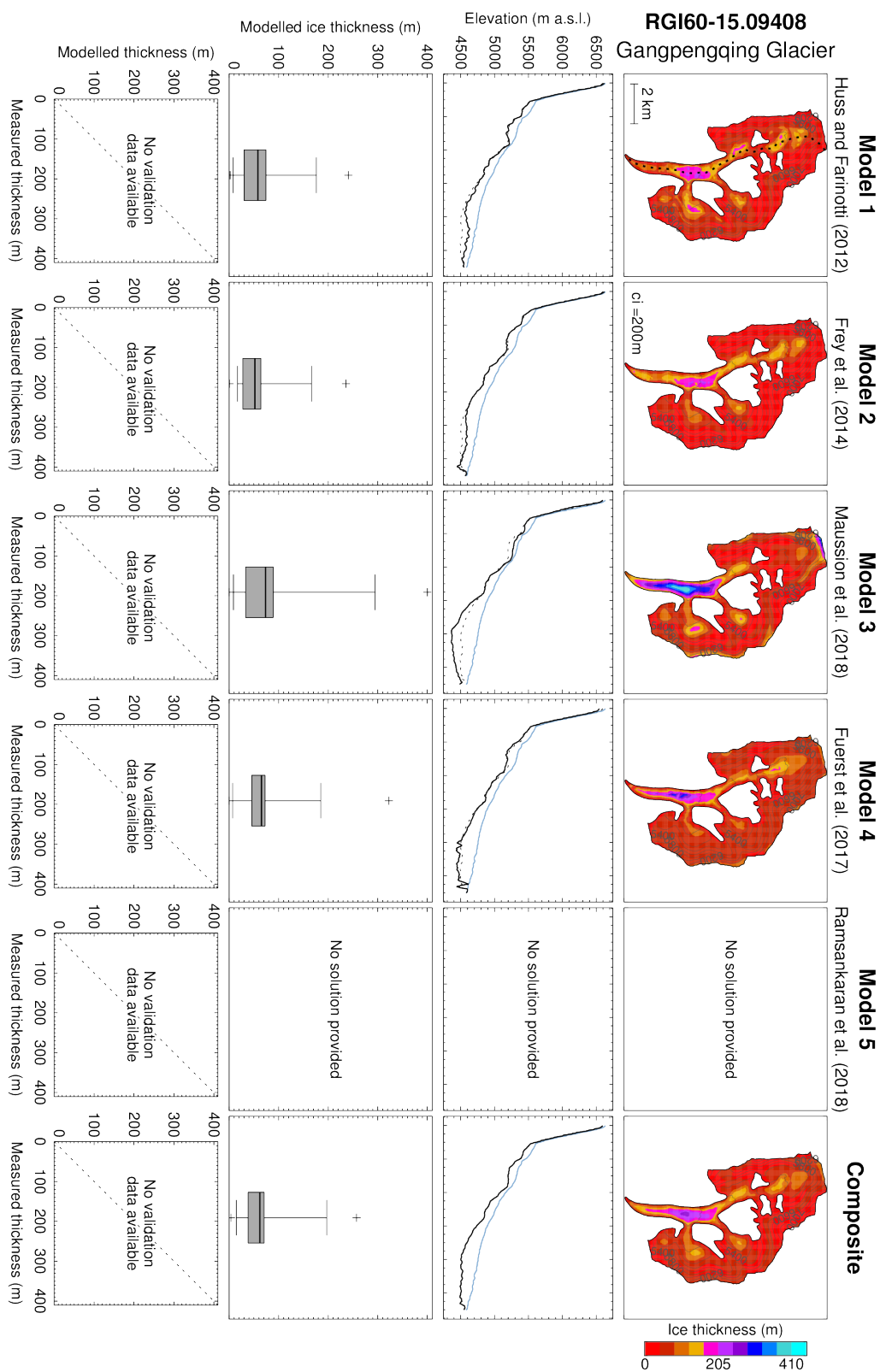


Figure S 21: Same as Figure S 7 but for glacier RGI60-15.09408 (RGI region "South Asia East").

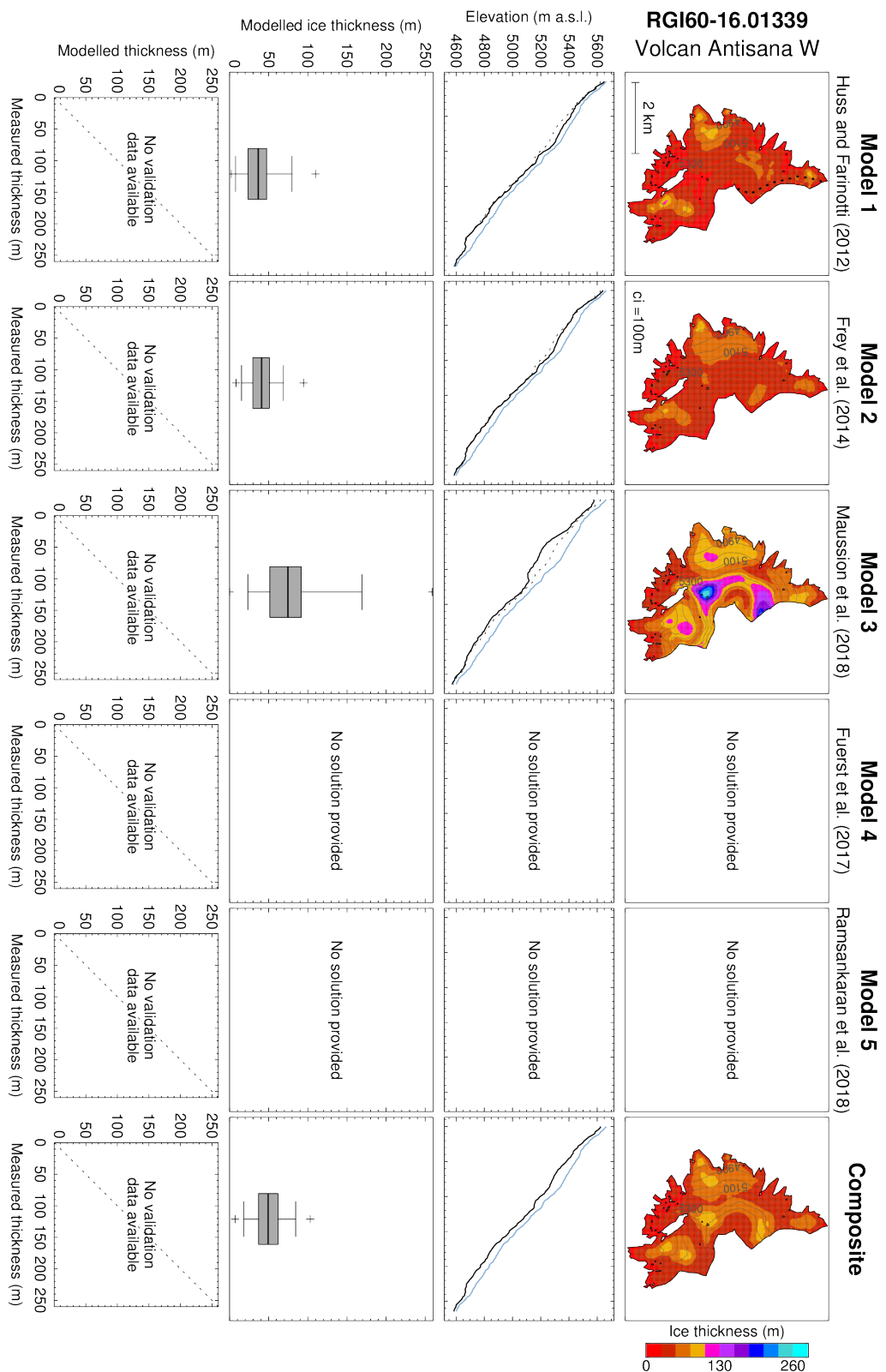


Figure S 22: Same as Figure S 7 but for glacier RGI60-16.01339 (RGI region "Low Latitudes").

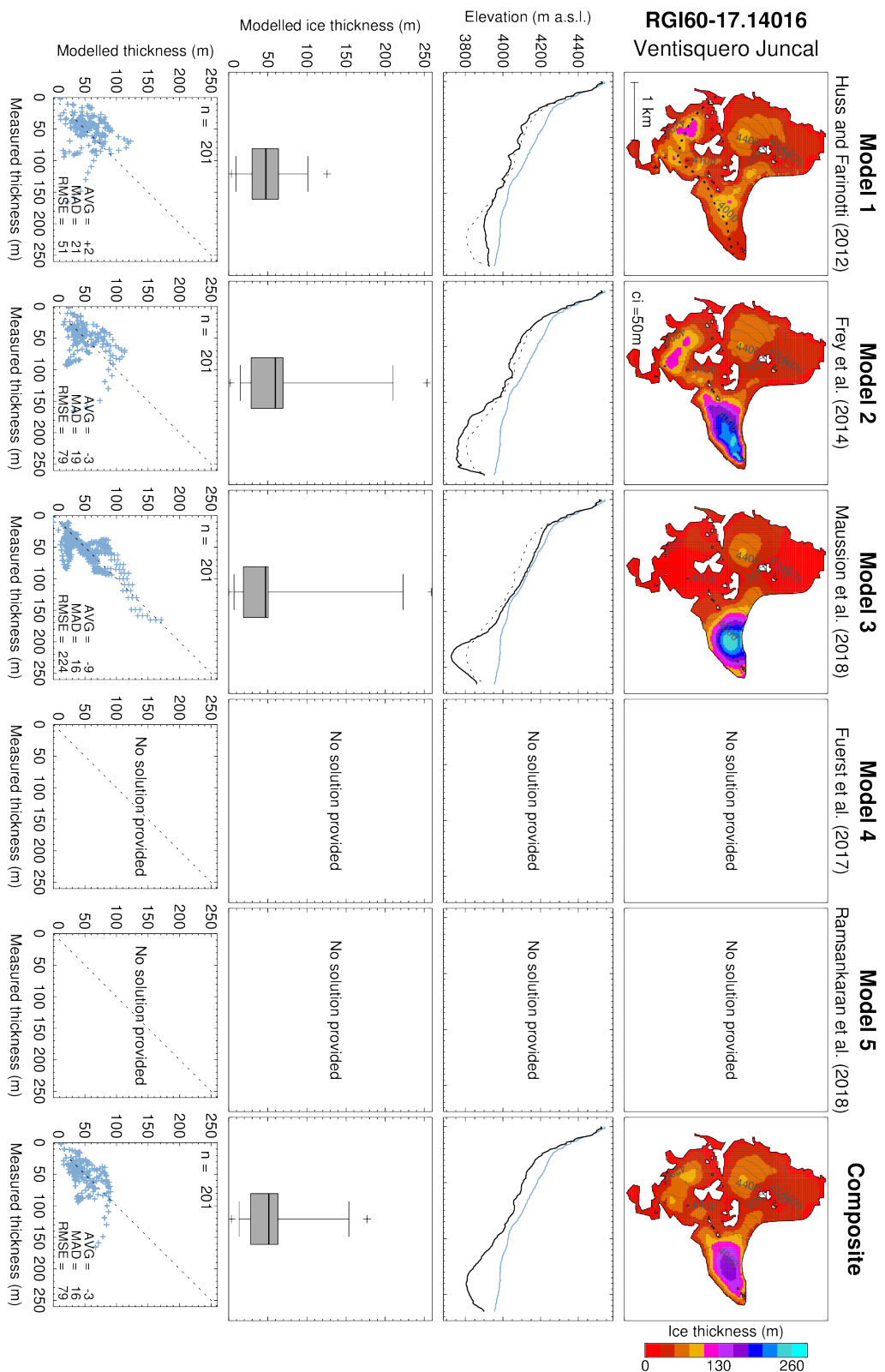
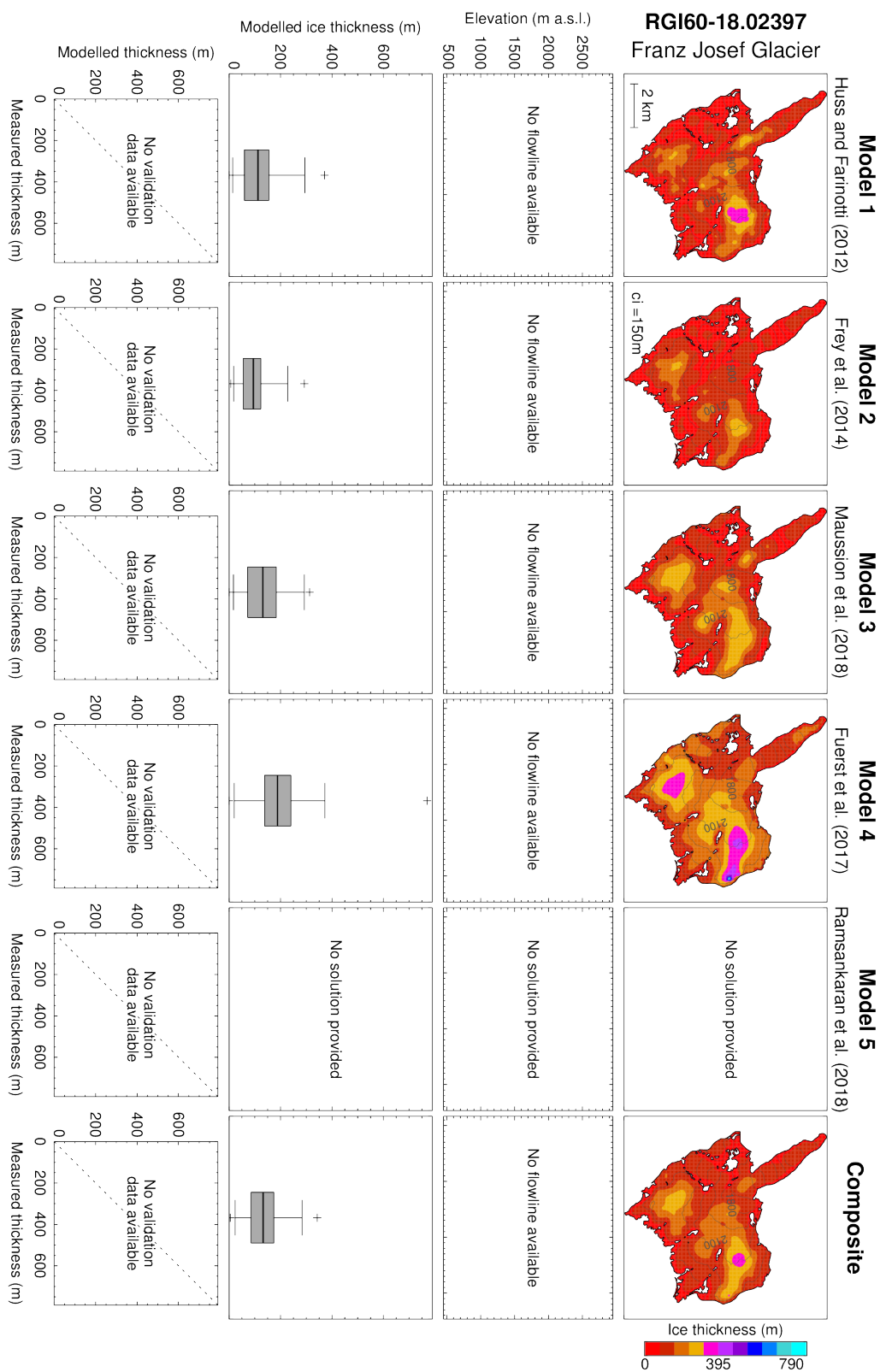


Figure S 23: Same as Figure S 7 but for glacier RGI60-17.14016 (RGI region "Southern Andes").



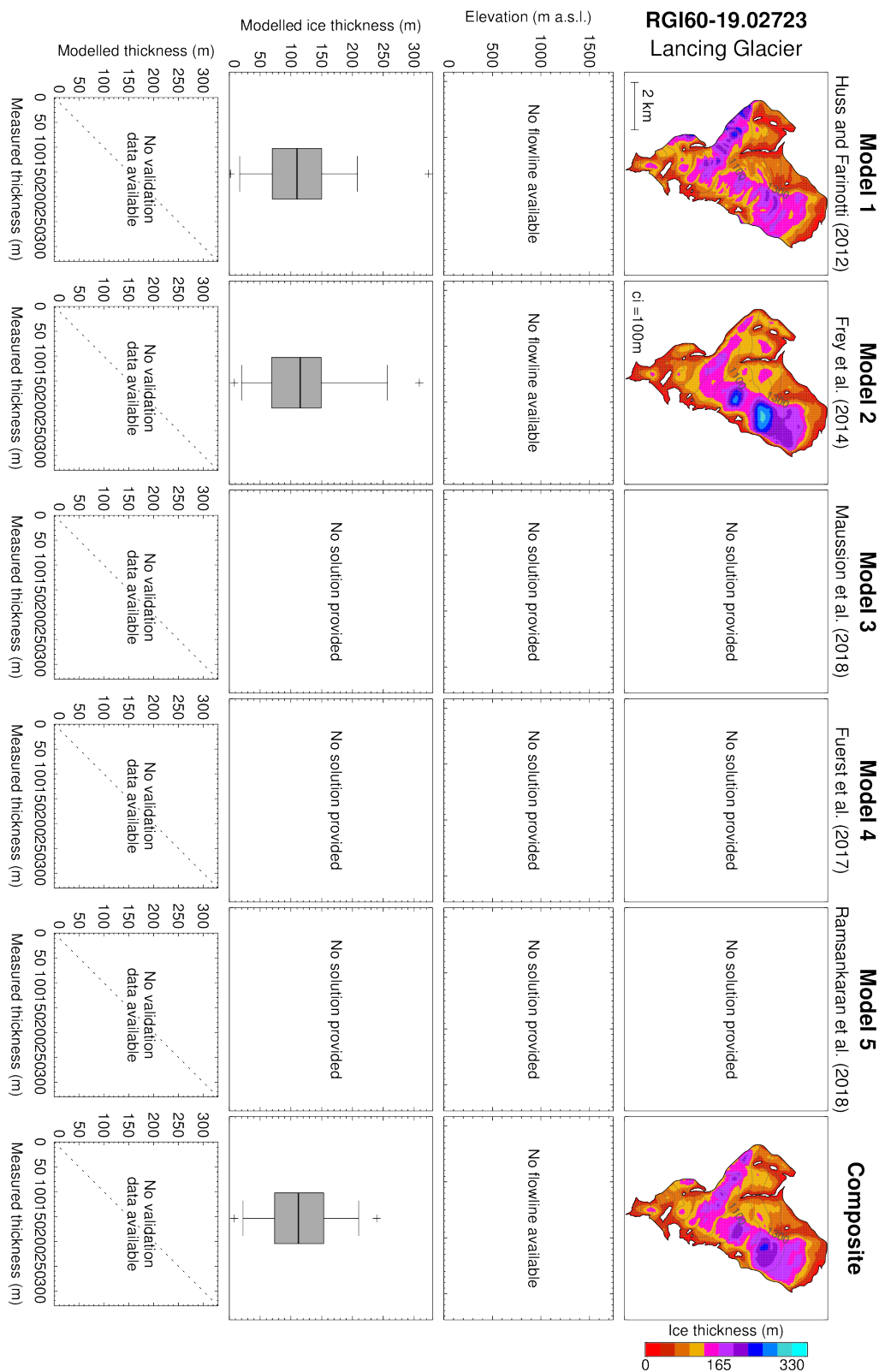


Figure S 25: Same as Figure S 7 but for glacier RGI60-19.02723 (RGI region "Antarctic and Subantarctic").

¹²⁶ **Supplementary References**

- ¹²⁷ Farinotti, D., Brinkerhoff, D. J., Clarke, G. K. C., Fürst, J. J., Frey, H., Gantayat, P., Gillet-
¹²⁸ Chaulet, F., Girard, C., Huss, M., Leclercq, P. W., Linsbauer, A., Machguth, H., Martin,
¹²⁹ C., Maussion, F., Morlighem, M., Mosbeux, C., Pandit, A., Portmann, A., Rabatel, A.,
¹³⁰ Ramsankaran, R., Reerink, T. J., Sanchez, O., Stentoft, P. A., Singh Kumari, S., van Pelt,
¹³¹ W. J. J., Anderson, B., Benham, T., Binder, D., Dowdeswell, J. A., Fischer, A., Helffricht,
¹³² K., Kutuzov, S., Lavrentiev, I., McNabb, R., Gudmundsson, G. H., Li, H., and Andreassen,
¹³³ L. M. (2017). How accurate are estimates of glacier ice thickness? Results from ITMIX, the
¹³⁴ Ice Thickness Models Intercomparison eXperiment. *The Cryosphere*, 11(2):949–970.
- ¹³⁵ Farinotti, D., Huss, M., Bauder, A., Funk, M., and Truffer, M. (2009). A method to estimate ice
¹³⁶ volume and ice thickness distribution of alpine glaciers. *Journal of Glaciology*, 55(191):422–
¹³⁷ 430.
- ¹³⁸ Frey, H., Machguth, H., Huss, M., Huggel, C., Bajracharya, S., Bolch, T., Kulkarni, A., Lins-
¹³⁹ bauer, A., Salzmann, N., and Stoffel, M. (2014). Estimating the volume of glaciers in the
¹⁴⁰ Himalayan–Karakoram region using different methods. *The Cryosphere*, 8(6):2313–2333.
- ¹⁴¹ Fürst, J., Navarro, F., Gillet-Chaulet, F., M., H., Moholdt, G., Fettweis, X., Lang, C., Seehaus,
¹⁴² T., Ai, S., Benham, T., Benn, D., Björnsson, H., Dowdeswell, J., Grabiec, M., Kohler, J.,
¹⁴³ Lavrentiev, I., Lindbäck, K., Melvold, K., Pettersson, R., Rippin, D., Saintenoy, A., Sánchez-
¹⁴⁴ Gámez, P., Schuler, T., Sevestre, H., Vasilenko, E., and Braun, M. (2018). The ice-free
¹⁴⁵ topography of Svalbard. *Geophysical Research Letters*.
- ¹⁴⁶ Fürst, J. J., Gillet-Chaulet, F., Benham, T. J., Dowdeswell, J. A., Grabiec, M., Navarro, F.,
¹⁴⁷ Pettersson, R., Moholdt, G., Nuth, C., Sass, B., Aas, K., Fettweis, X., Lang, C., Seehaus,
¹⁴⁸ T., and Braun, M. (2017). Application of a two-step approach for mapping ice thickness to
¹⁴⁹ various glacier types on Svalbard. *The Cryosphere*, 11(5):2003–2032.
- ¹⁵⁰ Glen, J. W. (1955). The creep of polycrystalline ice. *Proceedings of the Royal Society of London,*
¹⁵¹ Series A, 228(1175):519–538.
- ¹⁵² Grinsted, A. (2013). An estimate of global glacier volume. *The Cryosphere*, 7:141–151.
- ¹⁵³ Haeberli, W. and Hoelzle, M. (1995). Application of inventory data for estimating characteristics
¹⁵⁴ of and regional climate-change effects on mountain glaciers: a pilot study with the European
¹⁵⁵ Alps. *Annals of Glaciology*, 21:206–212.
- ¹⁵⁶ Harris, I., Jones, P. D., Osborn, T. J., and Lister, D. H. (2014). Updated high-resolution
¹⁵⁷ grids of monthly climatic observations the CRU TS3.10 Dataset. *International Journal of*
¹⁵⁸ *Climatology*, 34(3):623–642.
- ¹⁵⁹ Huss, M. and Farinotti, D. (2012). Distributed ice thickness and volume of all glaciers around
¹⁶⁰ the globe. *Journal of Geophysical Research*, 117:F04010.
- ¹⁶¹ Huss, M. and Hock, R. (2015). A new model for global glacier change and sea-level rise. *Frontiers*
¹⁶² in *Earth Science*, 3:Art. 54.
- ¹⁶³ Huss, M., Jouvet, G., Farinotti, D., and Bauder, A. (2010). Future high-mountain hydrology: a
¹⁶⁴ new parameterization of glacier retreat. *Hydrology and Earth System Sciences*, 14:815–829.

- 165 Kienholz, C., Rich, J. L., Arendt, A. A., and Hock, R. (2014). A new method for deriving glacier
166 centerlines applied to glaciers in Alaska and northwest Canada. *The Cryosphere*, 8(2):503–519.
- 167 Linsbauer, A., Paul, F., and Haeberli, W. (2012). Modeling glacier thickness distribution and
168 bed topography over entire mountain ranges with GlabTop: Application of a fast and robust
169 approach. *Journal of Geophysical Research*, 117:F03007.
- 170 Martín-Español, A., Navarro, F., Otero, J., Lapazaran, J., and Blaszczyk, M. (2015). Estimate
171 of the total volume of Svalbard glaciers, and their potential contribution to sea-level rise,
172 using new regionally based scaling relationships. *Journal of Glaciology*, 61(225):2941.
- 173 Marzeion, B., Jarosch, A., and Hofer, M. (2012). Past and future sea-level change from the
174 surface mass balance of glaciers. *The Cryosphere*, 6:1295–1322.
- 175 Maussion, F., Butenko, A., Eis, J., Fourteau, K., Jarosch, A. H., Landmann, J., Oesterle, F.,
176 Recinos, B., Rothenpieler, T., Vlug, A., Wild, C. T., and Marzeion, B. (2018). The Open
177 Global Glacier Model (OGGM) v1.0. *Geoscientific Model Development Discussions*, 2018:1–
178 33.
- 179 Meinshausen, M., Smith, S., Calvin, K., Daniel, J., Kainuma, M., Lamarque, J.-F., Matsumoto,
180 K., Montzka, S., Raper, S., Riahi, K., Thomson, A., Velders, G., and van Vuuren, D. (2011).
181 The RCP greenhouse gas concentrations and their extensions from 1765 to 2300. *Climatic
182 Change*, 109(1-2):213–241.
- 183 Paterson, W. S. B. (1994). *The Physics of Glaciers*. Pergamon, New York, third edition.
- 184 Radić, V., Bliss, A., Beedlow, A., Hock, R., Miles, E., and Cogley, J. (2014). Regional and global
185 projections of twenty-first century glacier mass changes in response to climate scenarios from
186 global climate models. *Climate Dynamics*, pages 1–22.
- 187 Radić, V. and Hock, R. (2010). Regional and global volumes of glaciers derived from statistical
188 upscaling of glacier inventory data. *Journal of Geophysical Research*, 115:F01010.
- 189 Ramsankaran, R., Pandit, A., and Azam, M. (2018). Spatially distributed ice-thickness mod-
190 elling for Chhota Shigri Glacier in western Himalayas, India. *International Journal of Remote
191 Sensing*, 39(10):3320–3343.
- 192 WGMS (2016). Glacier thickness database 2.0. I. Gärtner-Roer, L. M. Andreassen, E. Bjerre,
193 D. Farinotti, A. Fischer, M. Fischer, K. Helffricht, M. Huss, T. Knecht, S. Kutuzov, J. Land-
194 mann, I. Lavrentiev, H. Li, Z. Li, H. Machguth, K. Naegeli, F. Navarro, A. Rabatel, P. Stentoft,
195 M. Zemp (eds.), World Glacier Monitoring Service, Zurich, Switzerland.